

Studies on the Current Results of Mechanical and Vehicle Engineering Research at Széchenyi István University

Tanulmányok a Gépészeti és Járműmérnöki Kutatások Aktuális Eredményeiről a Széchenyi István Egyetemen

Széchenyi István Egyetem
Audi Hungaria Járműmérnöki Kar
“Járműmérnöki Kutatások” Konferencia

2018. május

Szerkesztette: Buruzs Adrienn

ISBN 978-615-5837-19-7

Content

D. Fülep: Applying Brenner formulas for constructing carbon nanostructures	2
D. Fülep: Inspection of the effect of neighbour distance in molecular dynamics simulations	10
J. Kun: Effect of Biot-parameter variations on acoustical simulations	16
F. Tancsics, T. Ibricsz: Researching of energy-saving material technologies and its current results	21
G. Monek: Expansion analysis of Fanuc Robot Cell	30
J. Kun: Review of FEM-PEM methods in thin walled structures	34
N.Szántó: Festo prolog factory simulation modelling	40
F. Hajdu: Numerical examination of simple nonlinear systems	44
H. Hargitai, N. Bíró: HDPE/PA hybrid nanocomposites	52
I. Hatos: Influence of DMLS parts building orientation on the part surface roughness	57
M. Pesthy, Cs. Tóth-Nagy, O. J. Richarz, B. B. Tóth: Condition Monitoring Method Development for Electric Motor Bearings with Vibration Analysis and Accelerated Aging Process	61
N. Kulcsár: Lifelike problems in mathematics lessons	68
A. Buruzs: Availability of rare earths and the need of the automotive industry	71
N. Szántó: Robot path generation from image recognition	76
G. Monek: Statistical Quality and Process Control with using R and Digital Twin	81
Á. I. Szabó, Cs. Tóth-Nagy: Experimental Investigation of the Friction Decreasing Effects of Nanosized C60 Fullerene Doped Engine Lubricant Performed on Oscillating Tribometer	85

Applying Brenner formulas for constructing carbon nanostructures

D. Fülep

Department of Mathematics and Computer Science, Széchenyi István
University
Győr, Hungary
e-mail: fulep@sze.hu

Abstract: This paper contains the description of a development and evaluation process in which Brenner formulas were adopted to study construction of 3D carbon nanostructures in self-organized way.

Keywords: molecular dynamics simulation, graphene nanoribbon, carbon nanotube, Brenner formulas

1. Introduction

Due to their extraordinary electric properties, producing carbon nanostructures has become a hot topic of research in the last years. [1-3]. Creating nanotubes and other three-dimensional nanostructures are under intensive theoretical and experimental study [4-5]. Besides experimental methods or instead of them, the rapid development of IT tools in this research field made it also possible for the researchers to use simulation methods looking for answers to their research questions [6].

Former research work has been done to motivate the production of nanostructures from graphene ribbons with investigating the conditions of production applying IT methods. [7-8]. This research work aims to apply new methods where physical-chemical exactitude, effectiveness and running speed are the main goals.

2. Methods: Applying Brenner algorithm

Due to Brenner formulas [9], we have the number of atoms N , R_0 coordinates and \mathbf{v}_0 initial speed vectors. Time step of simulation is Δt . Energy of each atom is the following:

$$E_i = \frac{1}{2} \sum_j E_{ij} \quad (1)$$

where E_{ij} is bonding energy between atom i and j , j values are the indices of the neighbors of atom i . Neighbors are atoms within the distance of 2 Å. Due to Brenner formulas, atomic bond energy can be written as follows:

$$E_{ij}(r) = E_R(r) - \overline{B_{ij}} E_A(r) \quad (2)$$

where r is the length of vector \vec{r}_{ij} (the distance of atom i and j).

$$r = |\vec{r}_{ij}| \quad (3)$$

E_R repulsive part of E_i :

$$E_R(r) = \frac{D_e}{S-1} e^{-\sqrt{2S}\beta(r-R_e)} \quad (4)$$

E_A attractive part of E_i :

$$E_A(r) = \frac{D_e S}{S-1} e^{-\sqrt{2/S}\beta(r-R_e)} \quad (5)$$

where D_e , S , β , R_e constants are Brenner parameters, and the:

$$\overline{B_{ij}} = \frac{B_{ij} + B_{ji}}{2} \quad (6)$$

where

$$B_{ij} = \left[1 + \sum_{k \neq i, j} G(\Theta_{ijk}) \right]^{-\delta} \quad (7)$$

where δ is parameter and

$$G(\Theta_{ijk}) = a_0 \left[1 + \frac{c_0^2}{d_0^2} - \frac{c_0^2}{d_0^2 + (1 + \cos(\Theta_{ijk}))^2} \right] \quad (8)$$

a_0 , c_0 , d_0 are parameters and Θ_{ijk} is angle between bonds of atoms i and j and i and k.

$$\Theta_{ijk} = \arccos\left(\frac{r_{jix} * r_{kix} + r_{jiy} * r_{kiy} + r_{jiz} * r_{kiz}}{\sqrt{r_{jix}^2 + r_{jiy}^2 + r_{jiz}^2} * \sqrt{r_{kix}^2 + r_{kiy}^2 + r_{kiz}^2}}\right) \quad (9)$$

Bonding force of each atom:

$$F = \frac{dE}{dr} \quad (10)$$

Bonding force is calculated by explicit Euler method.

$$F = \frac{E_{new} - E_{orig}}{\Delta r} \quad (11)$$

Acceleration vector can be calculated as

$$a = \frac{F}{m} \quad (12)$$

where m is the mass of each atom. New coordinates and speed vectors can be calculated as:

$$r_{new} = r_0 + v_0 t + \frac{a}{2} t^2 \quad (13)$$

$$v_{new} = v_0 + at \quad (14)$$

where $t = \Delta t$ time step is 0.7 fs.

The algorithm was first evaluated by calculating the energy of a flat graphene ribbon where bonding energy of the atoms is -7.44 eV. Fig. 1 shows one of the simplest input models used.

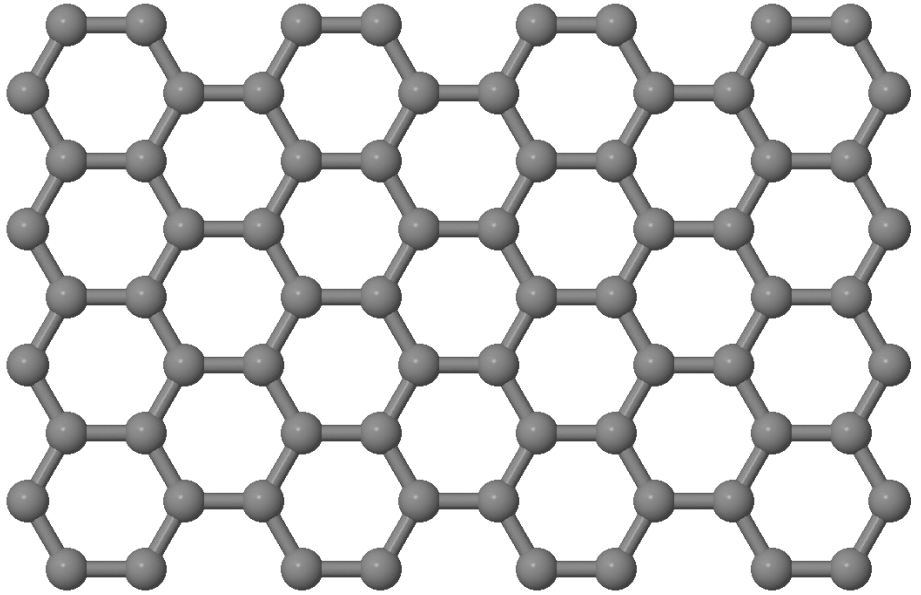


Figure 1.: Input model: flat graphene nanoribbon generated by software

Fig. 2 shows the energy of each atoms. Colors represent different energy levels - inner atoms of the structure are of -7.44 eV and atoms closer to the edges of the structures are higher.

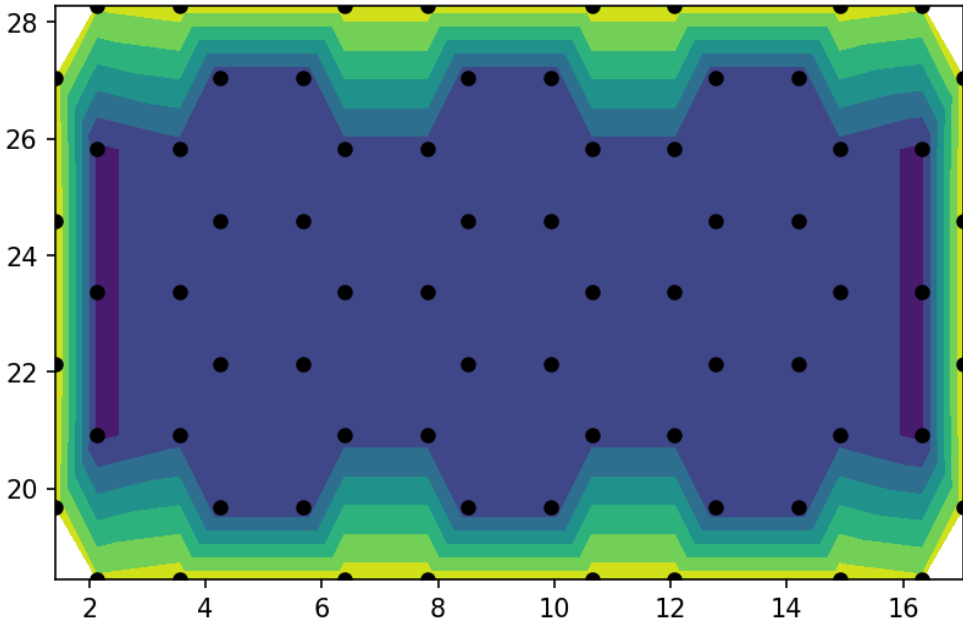


Figure 2. Energy of atoms of the model

On Fig. 3 the effect of initial random velocities can be seen as the speeds at the atoms are not exactly equal.

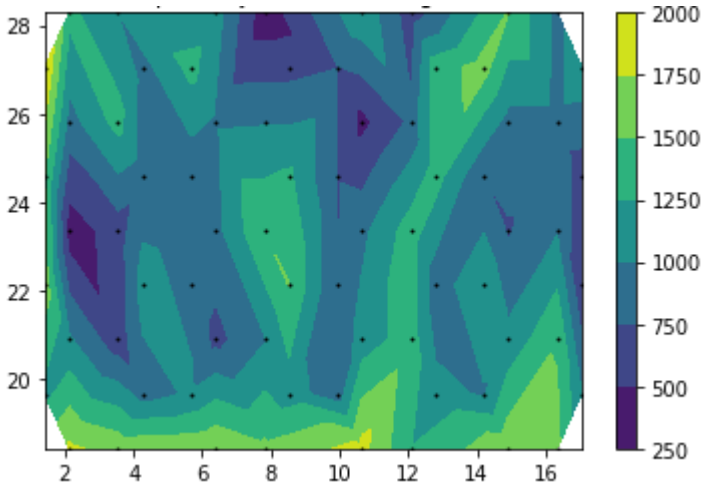


Figure 3. Atomic speed of model with 72 atoms.

Fig. 4. shows a larger model of 660 atoms where only one component of atomic speeds is visualized. Despite of random initial atomic movements, the speed values of the model are quite homogenous.

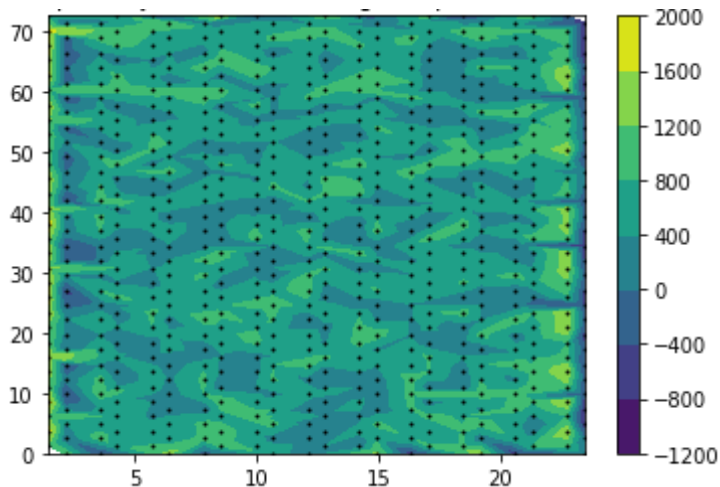


Figure 4. X component of atomic speed of a model with 660 atoms.

3. Acknowledgement

The author would like to thank to EFOP-3.6.1-16-2016-00017 ‘Internationalisation, initiatives to establish a new source of researchers and graduates, and development of knowledge and technological transfer as instruments of intelligent specialisations at Széchenyi István University’ for the support of the research.

4. References

1. Avouris P Molecular electronics with carbon nanotubes Acc. Chem. Res. 35 1026–34 (2002)
2. Keren K, Berman R S, Buchstab E, Sivan U and Braun E (2003) DNA-templated carbon nanotube field-effect transistor Science 302 1380–2
3. Tapasztó L, Dobrik G, Lambin P and Biro L P Tailoring the atomic structure of graphene nanoribbons by scanning tunneling microscope lithography Nat. Nanotechnol. 3 397–401 (2008)

4. László I and Zsoldos I Molecular dynamics simulation of carbon nanostructures: the C₆₀ buckminsterfullerene Phys. Status Solidi b 249 2616–9 (2012)
5. László I and Zsoldos I Molecular dynamics simulation of carbon nanostructures: the D_{5h} C₇₀ fullerene Physica E 56 427–30 (2014)
6. Fülep D, Zsoldos I and László I Topological and energetic conditions for lithographic production of carbon nanotubes from graphene J. Nanomater. 379563 (2015)
7. Dávid Fülep, Ibolya Zsoldos, István László Position Sensitivity Study in Molecular Dynamics Simulations of Self-Organized Development of 3D Nanostructures MATERIALS SCIENCE FORUM 885: pp. 216-221. (2017)
8. Dávid Fülep, Ibolya Zsoldos, István László Self-organizing Behavior of Y-junctions of Graphene Nanoribbons INTERNATIONAL JOURNAL OF ENGINEERING RESEARCH AND APPLICATIONS 7:(5) pp. 34-47. (2017)
9. Brenner DW. Empirical potential for hydrocarbons for use in simulating the chemical vapor deposition of diamond films. Phys Rev B Condens Matter. Nov 15;42(15):9458-9471. (1990)

Inspection of the effect of neighbour distance in molecular dynamics simulations

D. Fülep

Department of Mathematics and Computer Science, Széchenyi István
University
Győr, Hungary
e-mail: fulep@sze.hu

Abstract: This paper describes the experiences on a molecular dynamics simulation based on Brenner formulas used for self-construction of 3D carbon nanostructures. Determining the set of neighbours of each atom is of fundamental importance. This paper examines the effect of neighbourhood distances

Keywords: *molecular dynamics simulation, Brenner formulas, distance of atoms, neighbour atoms*

1. Introduction

Creating straight nanotubes and other three-dimensional nanostructures are under intensive theoretical and experimental study in the last years [1-2]. Rapid development of IT tools in this research field made it also possible for the researchers to use simulation methods looking for answers to their research questions [3]. Former research work has been done to motivate the production of nanostructures from graphene ribbons with investigating the conditions of production applying IT methods. [4-5]. This research work aims to evaluate Brenner formulas [6] whether they are adequate for simulation of self-organised constructions of carbon nanostructures. The main focus of this work is inspecting the effect of atomic distances and determining the set of neighbour atoms which are involved in calculations.

2. Considering Brenner algorithm neighbourhood distances

While using the algorithm, it is fundamental to determine the neighbour atoms of each atoms in the model. The way of determining neighbourhood influences further calculations. Farther neighbours have smaller effect on interaction between atoms, though. In practice, about 2 Å is a widely accepted distance. The problem is that with real models, independent from the exact value of this distance limit, some

skipping in energy values can occur. This is a serious problem as forces are calculated from the derivatives of energy:

$$F = \frac{dE}{dr} \tag{1}$$

where infinite slopes in function F can occur at points where energy has skipping points.

Fig. 1 shows a graphene sheet where an atom is displaced. Two neighbours of the displaced atom with exact distances are shown. While moving back to its energy minimized resting place, the indicated neighbour atom with the distance within 2 Å (0.197 nm = 0.197 Å) will suddenly fall out of the limit distance. At this point, as the total energy of the atoms are summarized by all the bonding energy of neighbour atoms, there will be a small but noticeable skip in total energy.

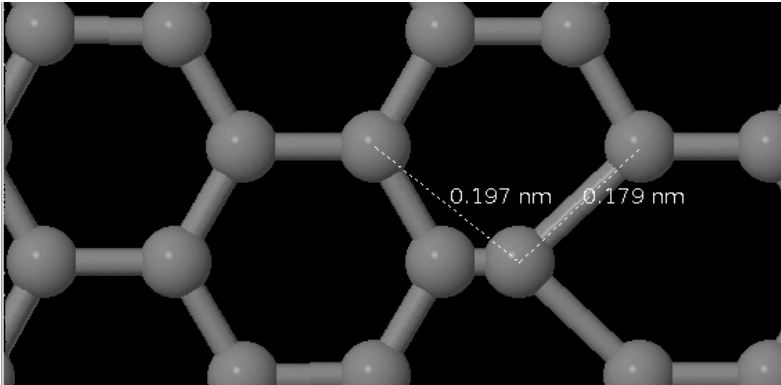


Figure 1. Flat graphene sheet with one displaced atom

This situation cannot be avoided by changing the limit value of 2 Å. For example, if we set limit to 1.8 Å, Fig. 2 shows a situation where a displaced atom will have a change in its cardinality of neighbourhood within some simulation steps.

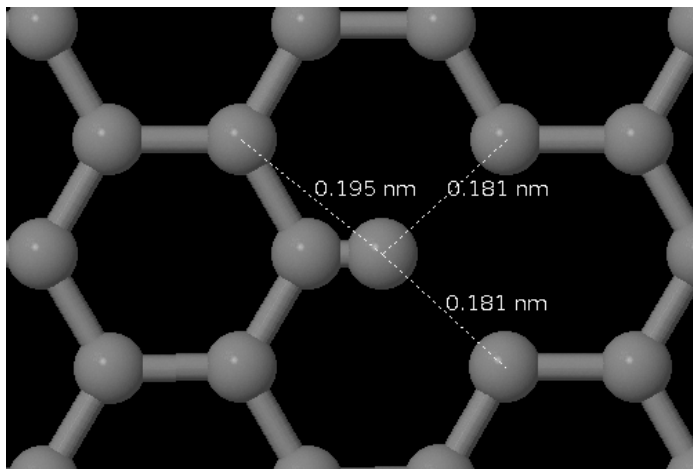


Figure 2. Graphene sheet with one displaced atom

Another serious problem can be shown on Fig. 2. If distance limit is set to 1.8 Å two atoms are not considered as neighbours but it is easy to understand a correct reconstruction of the structure needs that two atoms to act as neighbours.

These tests were also done with several other values between 1.7 Å and 6 Å and some atoms moving indistinctly on neighbour limit was found in each case. Illustratively, Fig 3. shows neighbour atoms in 5.8 Å of distance.

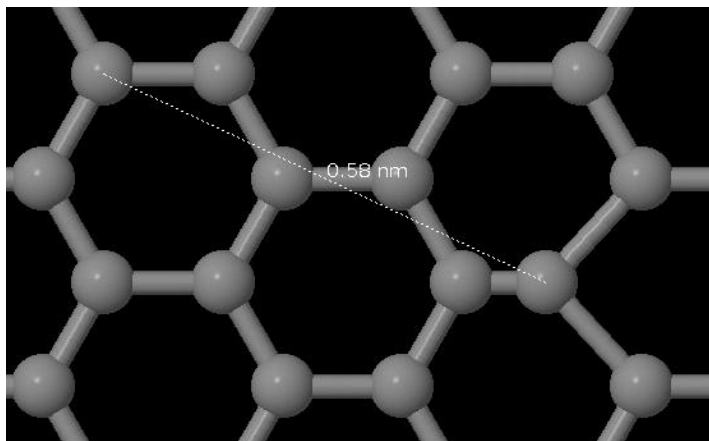


Figure 3. A neighbour atom in distance of 5.8 Å

Fig 4. shows the energy of a moving atom with neighbourhood limit set to 1.8 Å. At the skipping points atomic bond forces cannot be calculated. Similar charts can be drawn for larger limits but skipings are relatively smaller in singularity points.

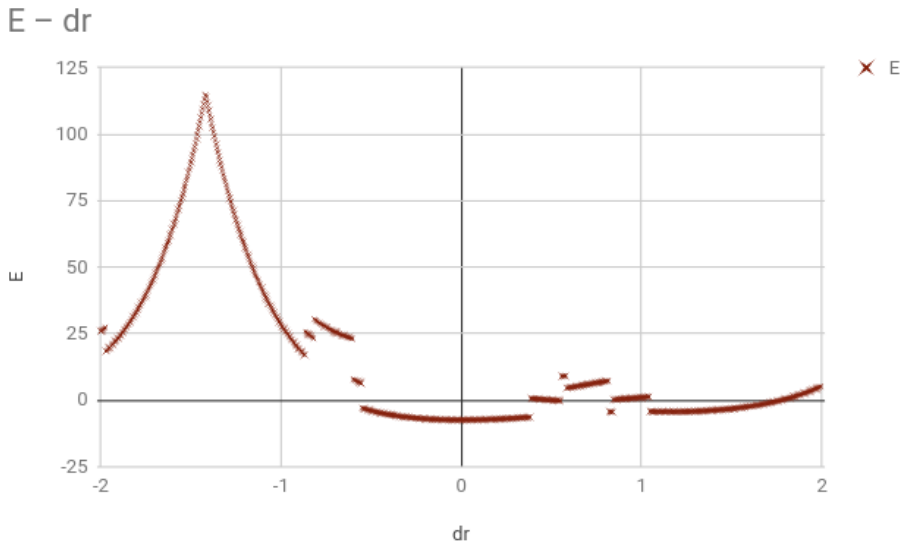


Figure 4. Atomic energy in the function of distance ($d=1.8 \text{ \AA}$)

Fig. 5 shows the effect of smoothing functions applied to handle the problem of singularities. Even applying the averaging smoothing functions several times, the skipping is quite large but starting manageable.

E és F

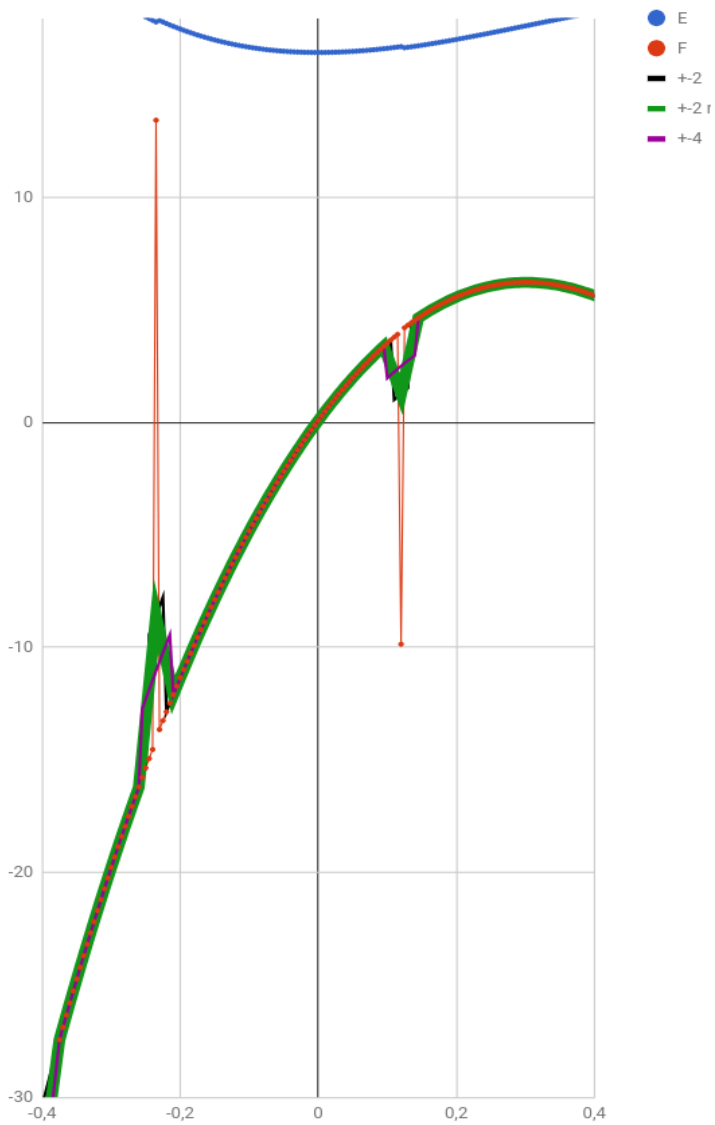


Figure 5. Effect of smoothing functions

Acknowledgement

The author would like to thank to EFOP-3.6.1-16-2016-00017 ‘Internationalisation, initiatives to establish a new source of researchers and graduates, and development of knowledge and technological transfer as instruments of intelligent specialisations at Széchenyi István University’ for the support of the research.

References

1. László I and Zsoldos I Molecular dynamics simulation of carbon nanostructures: the C60 buckminsterfullerene Phys. Status Solidi b 249 2616–9 (2012)
2. László I and Zsoldos I Molecular dynamics simulation of carbon nanostructures: the D5h C70 fullerene Physica E 56 427–30 (2014)
3. Fülep D, Zsoldos I and László I Topological and energetic conditions for lithographic production of carbon nanotubes from graphene J. Nanomater. 379563 (2015)
4. Dávid Fülep, Ibolya Zsoldos, István László Position Sensitivity Study in Molecular Dynamics Simulations of Self-Organized Development of 3D Nanostructures Materials Science Forum 885: pp. 216-221. (2017)
5. Dávid Fülep, Ibolya Zsoldos, István László Self-organizing Behavior of Y-junctions of Graphene Nanoribbons International Journal of Engineering Research and Applications 7:(5) pp. 34-47. (2017)
6. Brenner DW. Empirical potential for hydrocarbons for use in simulating the chemical vapor deposition of diamond films. Phys Rev B Condens Matter. Nov 15;42(15):9458-9471. (1990)

Effect of Biot-parameter variations on acoustical simulations

J. Kun

**Széchenyi István University, Department of Whole Vehicle Development
Egyetem tér 1., 9026 Győr, Hungary
e-mail: kun.janos@ga.sze.hu**

Abstract: This article summarizes concisely the importance of the Biot-theory in the field of acoustical simulations. Most relevant Biot parameters are introduced, in relation to their use in the vehicle industry. Measurement strategies for material validation are described. Their complexity and introduced effects on simulations are explained.

Keywords: Biot-parameters, poroelastic materials, acoustics, simulation

1. Introduction

Customer expectations are ever growing in the vehicle industry. To attract and even retain buyers and stay in business, manufacturers need their new models to surpass older ones in all aspects. Acoustics is a field where initial development opened up vast potentials: the earliest acoustically treated cars eliminated major noise sources like the engine and gearbox, only to find the noise levels of the HVAC unit to be disturbing passenger comfort. With the advent of electric drivetrains and their introduction of completely new baseline frequencies and sound pressure levels, even more advanced acoustic tools are necessary to be able to satisfy customer demand.

Intricate interior details and various sound-deadening materials are used in today's vehicles partly to create appealing interior designs as well as to reduce interior noise levels. These materials are generally plastics or some kinds of textile fibres, which are collectively called "trim" in the industry. As their impact on noise levels inside the cabin is quite profound, they should be modelled well in simulations. However, their complexity often makes this very difficult. In the following paragraphs, a principal theory is going to be introduced that can help simulations return even more accurate results.

2. Poroelastic materials

Trim elements belong to a larger cluster of materials, called poroelastic materials [1]. These substances consist of a solid matrix which encloses fluid-filled, interconnected cavities (pores). Both naturally occurring and man-made porous materials exist, with the following examples:

- Natural: biological tissues, various soil types
- Man-made: ceramics, foams, foamed plastics

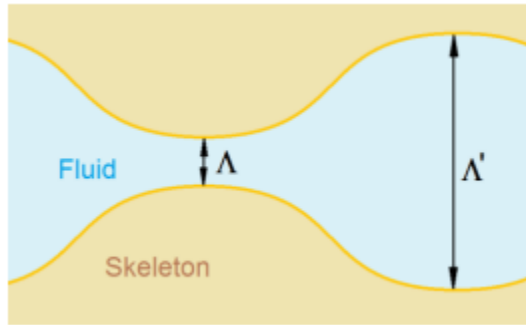


Figure 1.: cross-section of a generic poroelastic material [2]

Their significance lies in the fact that their influence on interior acoustics is highly important. Accurate mathematical modelling is essential to account for their effects.

3. Biot-theory

3.1 Introduction

Marcel Biot formulated the first version and the fundamentals of the Biot-theory in 1941, while the wave propagation inside a fluid-filled porous matrix was described first in 1956. The system of equations set up describes the two main variable vectors, namely the displacements of the fluid and the solid matrix in all directions. This set of equations still forms the basis of the Biot-models used today. In order to accurately represent the porous material effects, the Biot-theory relies on specific parameters [3].

3.2 Biot-parameters

As the interaction between the fluid-filled pores and the solid matrix is quite complex, Biot used various parameters to account for all the influencing factors of

the material for acoustic modelling. Overall, between 8 and 15 parameters are required, depending on which formulation of the equations is being used based on the available data. Parameters can be separated into two groups: parameters describing the phases (e.g. fluid density) and Biot-specific factors (e.g. tortuosity). Ideally, all are required and theoretically, they can be measured for simulations.

3.3 Biot-parameter measurement

To determine material qualities and fitness for purpose, Biot-parameters can be measured. However, their complicated nature means that not all of them can be measured directly. Therefore three measurement categories must be differentiated in order to be able to account for all required parameters [4]:

- Direct: as the name suggests, applicable for parameters that can be measured without intermediate methods (e.g. mechanical properties)
- Indirect: parameters gained using analytical-empirical methods on directly measurable quantities.
- Inverse: numerical measurement method, by way of minimizing a target function.

Very important to note for the indirect and inverse methods, that their errors largely depend on the actual analytical, empirical and numerical methods employed [5].

3.4 Biot-parameter effects

Unfortunately, the application of the Biot-theory is currently difficult in an industrial setting. The calculations become cumbersome and directly cannot be applied. However, the following graph of slow yet accurate simulations shows how much poroelastic materials influence acoustic response [6].

The test case for Figure 2. was a sample, simplified floor panel structure with a carpet-like material added. The graph shows the acceleration response for an excitation in a given point across a wide frequency band for two configurations: carpeted (TB, short for trimmed body) and non-carpeted (BIW, short for body-in-white) configurations. It is evident that the influence of the carpet cannot be neglected, and some model for the Biot-parameters is necessary. Modeling of Biot-theory is especially problematic due to the frequency dependency of parameters, however, novel methods can be used to overcome the complexity and yield accurate results in reasonable timeframes.

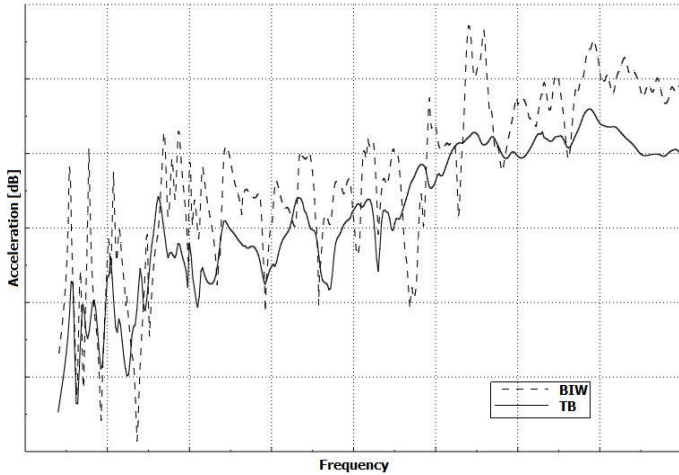


Figure 2.: Acceleration response of a sample floor with (TB) and without (BIW) poroelastic carpet material [7]

4. Summary

Poroelastic materials are essential to provide adequate passenger comfort in today's cars. To model their effect already in the design phase, Biot-theory is employed during acoustic simulations. Biot-theory describes poroelastic materials with various parameters. The goal for future simulation methods should be to employ a model that approaches the accuracy of the solution of the full Biot-theory equations, however requires much less time to solve to be implementable in strict development schedules.

Acknowledgement

The author would like to thank to EFOP-3.6.1-16-2016-00017 'Internationalisation, initiatives to establish a new source of researchers and graduates, and development of knowledge and technological transfer as instruments of intelligent specialisations at Széchenyi István University' for the support of the research.

References

1. Cameron, Christopher J., et al. "Prediction of NVH Behaviour of Trimmed Body Components in the Frequency Range 100–500Hz." *Applied Acoustics*, vol. 71, no. 8, 2010, pp. 708–721., doi:10.1016/j.apacoust.2010.03.002.
2. J.F. Allard and N. Atalla: Propagation of Sound in Porous Media, John Wiley & Sons Ltd. 2009. ISBN 978-0-470-746615-0
3. Olivier Dazel: Numerical methods for the Biot theory in acoustics, University of Maine – Le Mans
4. ISO 9053: International Organization for Standardization – Acoustics – Materials for acoustical applications – Determination for airflow resistance
5. Wolkesson, Martin. Evaluation of Impedance Tube Methods - A Two Microphone In-situ Method for Road Surfaces and the Three Microphone Transfer Function Method for Porous Materials. Thesis. Chalmers University of Technology, 2013. Göteborg: Division of Applied Acoustics, 2013. Print.
6. Kobayashi, Norimasa, et al. "Dynamic Behavior Analysis of Vehicle Acoustic Trim Using FEM." *The Journal of the Acoustical Society of America*, vol. 123, no. 5, 2008, pp. 3571–3571., doi:10.1121/1.2934644.
7. Sipos, Dávid, et al. "THE EFFECT OF THE BIOT-PARAMETERS ON THE DYNAMIC AND ACOUSTIC RESPONSE OF A VEHICLE ." 2018.

Researching of energy-saving material technologies and its current results

F. Tancsics¹, T. Ibriksz²

¹Széchenyi István University, Department of Material Sciences and Technology, 9026 Győr, Egyetem tér 1, Hungary
e-mail: tancsics@sze.hu

²Széchenyi István University, Department of Material Sciences and Technology, 9026 Győr, Egyetem tér 1, Hungary

Abstract: Automotive industry is a strategic branch of the Hungarian national economy. Nowadays, the production of forged automotive components, achievement of the technical features and geometrical integrating of functions are clearly tending towards development and application of procedures with high added value in the industry. Based on the above demands of the industry, our research aims at emphasizing the energy-saving technologies applicable under industrial circumstances vs. classical high energy consuming technological procedures. The current goal of EFOP supported researches are to find industrial solution for technology of QST (Quenching and Self-Tempering) treatment in the forging industry, and to increase tool lifetime by using correct heat transfer coefficient in FEM (Finite Element Method) solver.

Keywords: forging, QST, lubricant, heat transfer coefficient, FEM

1. QST treatment research at the forging field

After direct quenching from final forming temperature, internal heat capacity of the workpiece can be used to self-tempering. If the steel composition is properly specified, the operation of classical quenching and tempering can be omitted. This technology has been successfully applied at rolling of profile iron for years, but at forging field it is a new technology [1][2]. In case of spindles that are installed into BPW axles it was a particular innovative requirement. During our research the mechanical properties of the classical heat treated spindles forged from S355J2 (EN10025-2: 2004) steel had to be approached with directional cooling of modifiable S460N structural steel.

As a first step, we narrowed the area of the mechanical problems generated by the new process. The S460N structural steel was modified in composition within the tolerance range for the good of strength-enhancing ingredients. We have created the special, strengthened version of S460N steel and named it S460R steel. The development of strength was explained by two factors. On the one hand, there was a requirement of an original minimum surface hardness to preserve the wear resistance (this almost immediately excluded the use of air cooling) and on the other hand we wanted to increase the initial stress level of the fatigue failure.

The following real challenge was to define the toughness characteristics (elongation and Charpy test). The workpieces, which were cooled by the calm air from the final forging temperature, were dipped in water with suitable temperature and heat-absorbing ability for several seconds. Subsequently, the workpieces were cooled by the calm air, which provided the proper material structure utilizing the impact of the Self-Tempering (Fig. 1). In fact, the appropriate material structure was calibrated for the sampling environment, taking the machining requirements into account.



Figure 1. On the left side of the figure the forged spindle can be seen. On the right side of the figure the main stages of cooling process can be seen (starting point shown by arrow)

For this period of our research we made the following findings:

- The required 27 J Charpy test value in the 16-18% elongation interval at -20 °C can be achieved if the dipping temperature is below 900 °C. All this is confirmed by the results shown in Figure 2.
- We have found some technological parameters to fulfill the DP material structure in the area of sampling referring to spindle made of S460R steel. The DP (Dual Phase) structure consisted of a coarsened ferrite (F^P) and fine bainite (B) as Figure 3 shows.

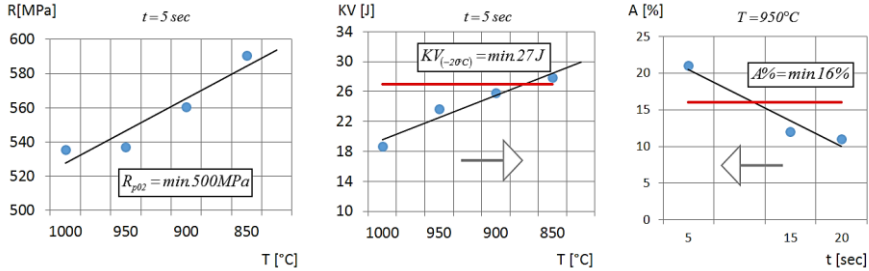


Figure 2. At the top side of the figure the results of strength after QST treating can be seen. At the bottom side of the figure the results of elongation after QST treating can be seen

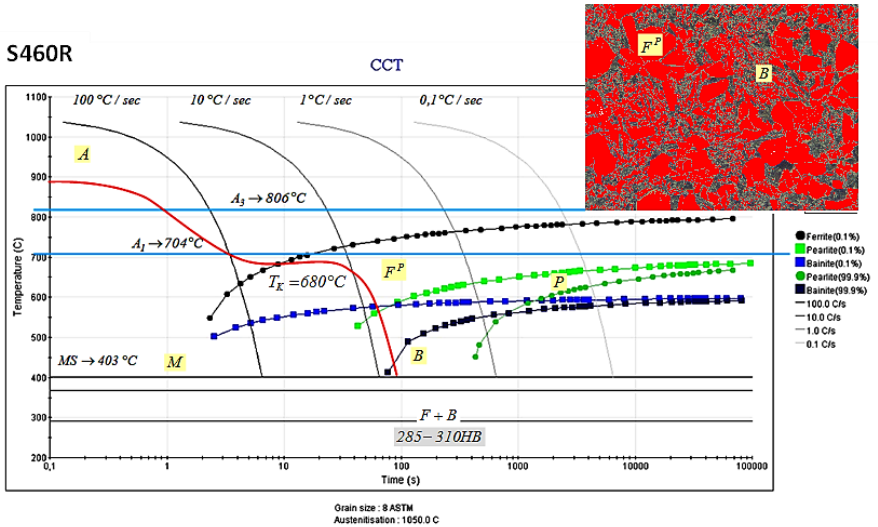


Figure 3. At the top side of the figure the results of strength after QST treating can be seen. At the bottom side of the figure the results of elongation after QST treating can be seen

The appropriate technological parameters will be used in the future as a boundary condition for FEM analysis and model experiments to specify and generalize the QST technology.

2. Explanation of heat transfer coefficient for FEM analysis at forging

Heat transfer between the forging tool and the working piece basically depends on a heterogeneous media, which contains large amount of oxide particles and solid lubricant mixed with graphite [3]. Knowing the technical properties of this media makes it possible to design wear process of the forging tools and the temperature on the surface of forged pieces. The latter is an important input data for modeling QST treating as well.

On the one hand the actuality of the lubrication test is provided by deceleration needs of the forging tool wear and the correct selection needs of heat transfer factor for FEM analysis. On the other hand, referring to graphite-based lubricants, the amount of mined graphite will be reduced in the future and currently the synthetically produced graphite is too expensive to replace it [4].

2.1 The graphite layer thickness

In the lubrication tests, the relationship between the Kudo's friction number (m) and the lubricant thickness layer was determined by an SU (Simple Upsetting) method with using lubricants diluted in different ratio. All this was necessary because the FEM analysis requires a friction number for forging simulations.

During evaluation of test pieces we used a Mathcad algorithm based on UBET (Upper-Bound Elemental Technique) method [5][6].

The layer thickness of solid lubricant sprayed on the tool surface was determined using function (1) based on the atomization technology and geometry data of the tool [7].

$$m_F = c_{SZ} \cdot q_V \cdot \eta \int_{t_K}^{t_T} dt, \quad (1)$$

whereabouts: m_F the mass of the solid lubricant sprayed onto the tool surface [mg], c_{SZ} % by weight of solid lubricant in the suspension [mg/cm³], q_V volumetric flow rate of the sprayed suspension per time unit [cm³/sec], η the efficiency of spraying (lubricant loss at lubricant deposition and at vaporization) [-], t_K the time to reach initial temperature of the adhesion [sec], t_T the total duration of spraying [sec].

The graphite content of the different types of lubricant (mined graphite based and synthetic graphite based) was determined by EDS (Energy Dispersive Spectroscopy) method. The results of the tests are summarized in Figure 4.

For this period of our research we made the following findings:

- The friction factors are nearly the same. This is possible if the amount of graphite content is nearly the same in the solid lubricant. This is shown in Figure 4.

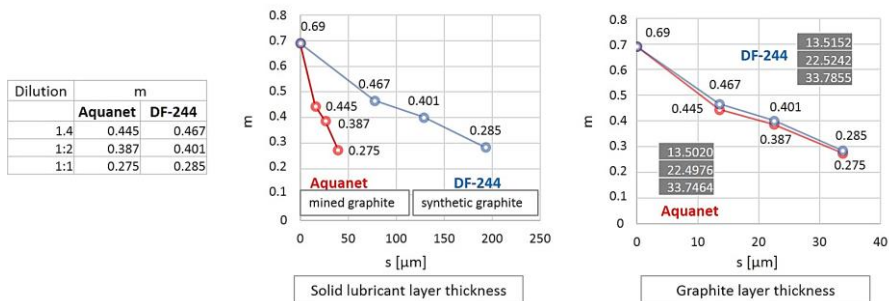


Figure 4. On the left side of the figure the solid lubricant content can be seen at different types of lubricant. On the right side of the figure the graphite content can be seen at different types of lubricant

- Lubricants containing synthetic graphite can provide an effective lubrication at higher dilution as well. Based on our experience, if the mined graphite based lubricant is diluted 1:2 (one part lubricant, two parts water), we get the same result as if the synthetic graphite based lubricant were diluted to 1:5. This is usually assisted by the smaller grain size of synthetic graphite as well.

2.2 The oxide scale layer thickness

During heating of steel, a multilayered oxide scale coating on the surface grows up. From substrate in sequence the layers on the steel surface are as follows: wüstit - magnetite - hematite. The formation features and thickness of the oxides basically depend on diffusion processes of the different composition layers. Temperature is the most important parameter of the thickness of the oxide layer since the constant value of the thermal diffusion rate per layer follows the Arrhenius law [8]. To determine the full thickness of the oxide scale layer, we used the function of J. Paidassi which was corrected by us per features of induction heating (2) [9].

$$x (\mu m) = 24550 \cdot \exp(-84650 / RT) \cdot \sqrt{t - 60(s)}, \quad (2)$$

whereabouts: x the instantaneous thickness of the oxide layer [μm], R the universal gas constant [J/molK], T the heating temperature expressed in Kelvin

[K], t the duration of oxidation (technical data of equipment and bars are needed) [sec].

Correlation (2) for the determination of the oxide scale layer thickness can be considered as appropriate by our measured data and the data of other literature [10].

At induction heating, the end surfaces of bars are exposed to greater heat, so in this case correlation (2) needs to be corrected with the value of increased temperature. Figure 5 shows the data of the measurements supporting the theoretical calculations (2).

Counterblow hammer	Induction heater	P [kg/h]	L (heater) [mm]	m (bar) [kg]	L (bar) [mm]	a (bar) [mm]	η [%]	T (bar) [°C]	x (oxide) [μm]
400 KJ	AEG	5000	8500	106.5	1500	B96	96	1273	160.8

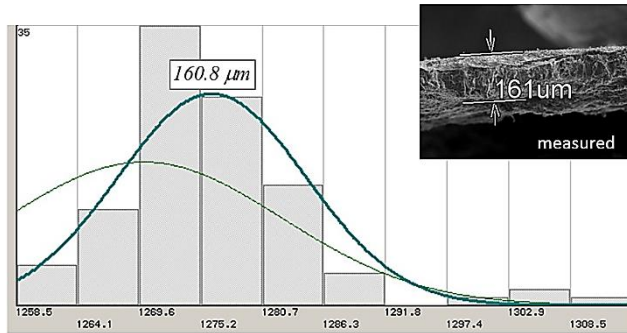


Figure 5. At the right top corner of the diagram the measured thickness of the oxide sample at 1275 °C can be seen. The diagram shows the distribution of measured temperatures referring to 35 pieces

2.3 The heat transfer coefficient for FEM analysis

The heat transfer can be characterized by the heat transfer coefficient. The heat transfer coefficient of the layer is the aggregate heat transfer coefficient of the components constituting the mixture (3) [11].

$$h_c = \frac{1}{\sum_{i=1}^n \left(\frac{x}{\lambda} \right)_i}, \quad (3)$$

whereabouts: h_c the heat transfer coefficient [W/m²K], x the thickness of each layer [m], λ the thermal conductivity of each layer [W/mK].

Preserving the layered structure of the media is boundary condition for application of relation (3) that can hold on its continuity during forging.

Figure 6 shows possible heat transfer coefficients between the tool surface and the workpiece, taking the thickness of the graphite layer at constant value into account: $x = 22.5 \mu\text{m}$.

It can also be seen, at constant graphite layer thicknesses, that the oxide layers with different thicknesses cause different degrees of contact pressures on the forging tool surfaces.

The CAD model about the FEM analysed forged piece can be seen next to the diagram.

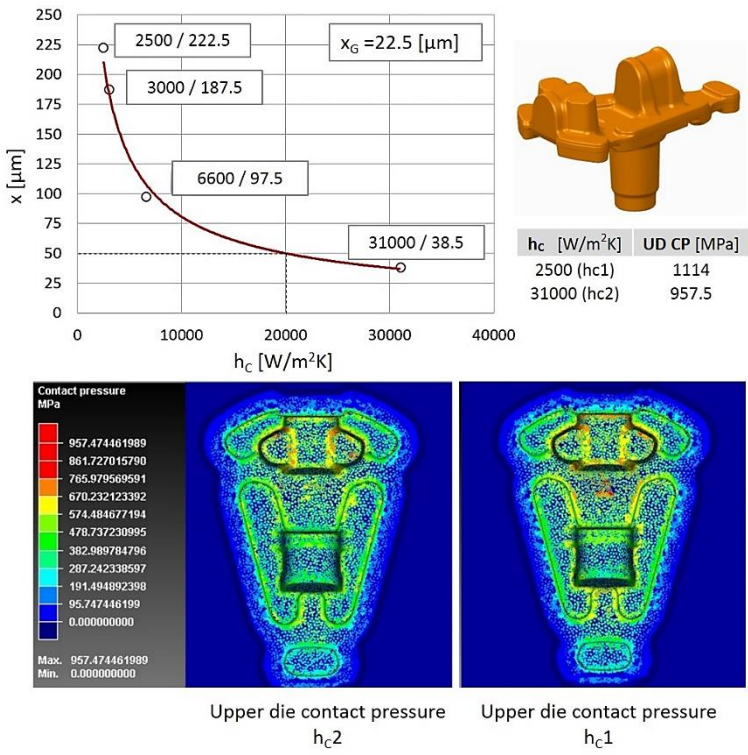


Figure 5. At the top side of the figure the results of heat transfer coefficients depending on the friction number can be seen. At the bottom side of the figure the results of contact pressure with different set-up parameters can be seen

Therefore knowing the suitable heat transfer coefficient, the descaling method and the lubricating systems is important.

For this period of our research we made the following findings:

- The effects of lubrication and oxidation processes have been made visible for FEM analysis
- The method provides the option to set the forging end temperature for QST treatment
- The diagram gives a good approximation selecting required heat transfer coefficient in range of heating temperature 1170-1300 ° C and 1.5 -105 kg range of forged mass

3. Summary and discussion

Summarizing our work, the goals basically are fulfilled for industrial applications, but the relationship of the heat transport processes under investigation needs to be clarified in laboratory conditions. We have selected the suitable parameters which influence the process. In the next stage of our work, we will examine the relationship of these parameters through simplified models and FEM analysis.

Priority issues will be: surface contamination (oxide, graphite), surface / volume ratio, complexity of geometry, heat transfer on the surface, temperature spread and distribution in the workpiece.

The relationship between local wear factor and geometry complexity depending on the thickness of the scale requires a separate examination.

Acknowledgement

The authors would like to thank to EFOP-3.6.1-16-2016-00017 'Internationalisation, initiatives to establish a new source of researchers and graduates, and development of knowledge and technological transfer as instruments of intelligent specialisations at Széchenyi István University' for the support of the research.

References

1. Y. Ishikawa ed., Online Quenched and Self-Tempered High Strength Steels, JFE Technical Report No.15 (May 2010) pp. 38-40.
2. Z. Bo et al., Research on a New Process of The Non-Quenched and Tempered Steel with High Strength and High Toughness, ScienceDirect, Physics Procedia 50 (2013) pp. 25-31.

3. F. Tancsics, T. Ibriksz, Gy. Kocsis, Investigation of the Relationship between Lubricant Layer and The Heat Transport at Hot Impression Die Forging, XVI. Képlékenyalakító konferencia, Miskolc, 2018, pp. 20-29, in Hungarian.
4. R. Spencer, L. Hill, A Flake's Chance in Cell: Quantifying Graphite Demand, Specialty Minerals & Metals, Industry Overview Nov 20th (2016), 35.
5. F. Tancsics, Practical Application of Virtual Forging Technologies, GlobeEdit, Saarbrücken, 2016, in Hungarian.
6. F. Tancsics, E. Halbritter, Determination of Friction Coefficient During Upsetting Using a Kinematically Admissible Velocity Field, Strojnícky Časopis, Journal of Mechanical Engineering, Vol.63 No.4, (2012), pp.197-223.
7. P.F. Mendez et al., Influence of Heat Transfer on The Application of Solid Lubricant on Hot Dies, Elsevier Scripta Materialia, Vol.59, No.7, (2008), pp.784-787.
8. L. Suarez et al., High Temperature Oxidation of Ultra-Low-Carbon Steel, Defect and Diffusion Forum Vols. 258-260, (2006), pp. 158-163.
9. B. Mašek et al., Influence of The Chemical Composition of 20MoCrS4 and Low-alloyed TRIP Steel on The Intensity of High Temperature Corrosion, Materials and Corrosion, V.58, I.9, (2007), pp.704–709.
10. E. Rie et al., Thermal Diffusivity Measurement of Oxide Scale Formed on Steel during Hot-rolling Process, ISIJ International, Vol.54, No.9, (2014), pp.2084–2088.
11. Y. Nobuki et al., Modeling of Heat Transfer Coefficient of Oxide Scale in Hot Forging, Science Direct, Procedia Engineering 81, (2014), pp.492 – 497.

Expansion analysis of Fanuc Robot Cell

G. Monek

Széchenyi István University, Department of Automobil Production
Technology
H-9026 Győr, Egyetem tér 1. Hungary
monek.gergo@sze.hu

Abstract: This paper contains the functional and technical description of the Fanuc robot cell. The expandability analysis of cellular components and the current communication architecture are presented. Furthermore, the integration of the cell into the i4.0-based system will be investigated.

Keywords: Fanuc, robot cell, I4.0

1. Introduction

The expandability test was carried out to meet the requirements of I4.0. The cell is a component of a sample board where different technology-level elements communicate with each other and work together to form a smart factory. Therefore, the main goal is to integrate into the system, to develop a communication protocol between older and new types of devices. Another goal is to create real-time interventions, higher-level control (MES - Manufacturing Execution System), and extract data generated during system operation, system monitoring and forecasting.[1,2]

2. Description of the FANUC cell at SZE

The robot cell contains two FANUC Mi-10A robots, one Mitsubishi PLC, two-level conveyor track and a camera control unit (Figure 1). The robot cell is located in a 3x3.5m area surrounded by 4mm Plexiglas. The robot systems include four emergency switches, which result in an immediate shutdown of both robots and four additional switches that can separately stop the robots.

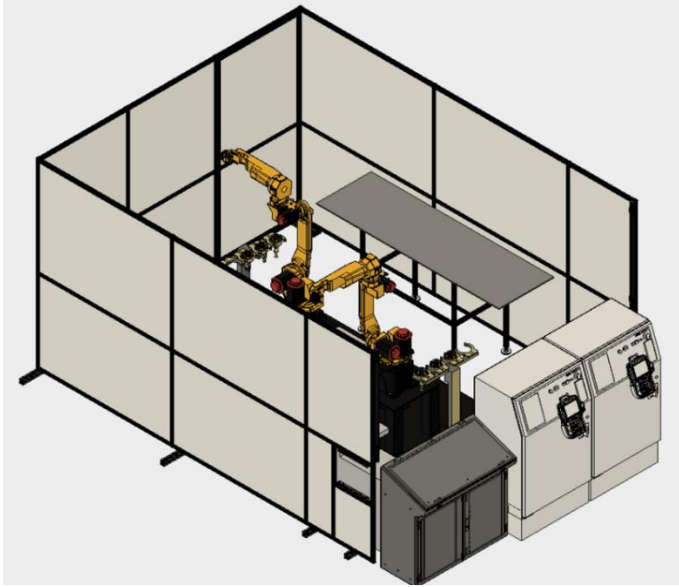


Figure 1. FANUC robotic cell (CAD model)

The Mitsubishi PLC carries out the operation of the cell and the corresponding HMI (human-machine interface) built into the control cabinet setting the parameters for operation. The PLC uses a 24V In / Out card to communicate with the two robots of the cell. Currently, all the input and output feet are occupied, they perform the task required to operate.

The main parameters of the FANUC M-10iA:

- 6 controlled axis
- maximum load capacity at wrist: 10 kg
- maximum reach: 1420 mm
- all axes have software-, electric- and mechanical brakes
- mechanical weight: 130 kg
- footprint: 283x283 mm [1]

3. Expandability analysis

Traditionally, there is no flow of information between the cell and the other constituents during operation, just a few data can be extracted from the processes, and the intervening process is not solved.

During the expansion, a PROFIBUS expansion card is added to the robot controllers (Figure 2), which allows the existing Siemens S7-1500 PLC to communicate with the robots, in this way removing the original Mitsubishi PLC. The advantage of Siemens PLC is that it can also communicate OPC, OPC UA and Node-RED so that other system components are available.

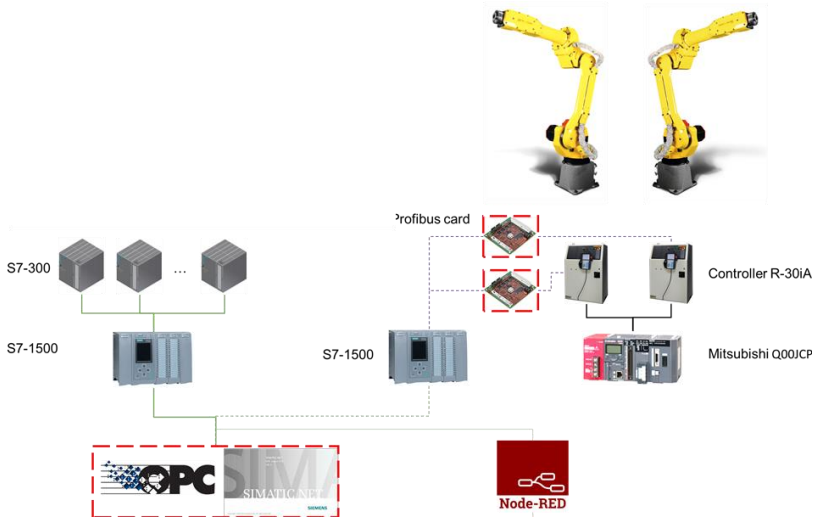


Figure 2. An outline of a possible architecture

The advantage of expanding the flow of information between the cell and other constituents can be obtained, a detailed set of information about processes can be obtained and the intervention in the process is ensured. Two-way communication is realized, which is a precondition for creating a Digital Twin. Without the complete replacement of devices, integration into the I4.0 system can only be achieved by extensions.

4. Summary

The system's resources make it possible to simulate the current technology level in the industry. Analysing and testing the possibilities of joining the system to an Industry4.0 environment. By replacing Mitsubishi PLC with Siemens and improving the communication of robots, it enables online monitoring and simulation of cell events in Plant Simulation and Process Simulation software's. With this modifications and opportunity the using NodeRED the robots can work with the other automated workstations in the research lab and the AGVs.

Acknowledgement

The authors would like to thank to EFOP-3.6.1-16-2016-00017 'Internationalisation, initiatives to establish a new source of researchers and graduates, and development of knowledge and technological transfer as instruments of intelligent specialisations at Széchenyi István University' for the support of the research.

References

1. D. Mourtzis, E. Vlachou, G. Dimitrakopoulos, V. Zogopoulos.: Cyber-Physical Systems and Education 4.0 – The Teaching Factory 4.0 Concept, *Procedia Manufacturing* 23., 2018, pp.129-134
2. Fanuc America Inc.:Fanuc M10-iA-Series Manual, Fanuc Robotics, 2008

Review of FEM-PEM methods in thin walled structures

J. Kun

**Széchenyi István University, Department of Whole Vehicle Development
Egyetem tér 1., 9026 Győr, Hungary
e-mail: kun.janos@ga.sze.hu**

Abstract: Current paper summarizes select articles on various methods to incorporate poroelastic materials into acoustic simulations. A short introduction to using poroelastic materials in simulations will be provided. Afterwards, three selected papers will be concisely summarized with their key findings and proven methods.

Keywords: Vehicle acoustics, poroelastic materials, FEA, simulation

1. Introduction

Poroelastic materials in general are materials that consist of a solid matrix which encloses fluid-filled, interconnected cavities (pores). Their importance in the automotive industry is that interior acoustic materials, such as carpeting, insulators, damping materials and all interior plastics (door cards, instrument panels, headliners, etc.) are made of porous material. As their influence on the sound pressure levels and acoustic behaviour inside the passenger cavity is very significant, they have to be accounted for during vehicle development. Ideally, simulation methods should be able to capture their effect as this would save costs downstream in the development cycle by reducing the number of physical prototypes to be built.

However, mathematically describing the poroelastic materials (PEM) is quite expensive in computation time. Biot-theory, the mathematical background behind PEM leads to extended simulation times, which makes it difficult to use in industrial development processes. Therefore manufacturers experimented with various models to account for the effect of PEM without explicit calculation of the Biot-equations.

Three papers are highlighted in this summary that contain techniques to include PEM in acoustic simulations. The basic acoustic simulation that PEM is going to be combined with is finite element analysis (FEA). FEA is generally used for structural calculations, however, after calculating displacements of a car body, a

coupled vibro-acoustic simulation can determine sound pressure levels (SPLs) within the discretized interior cavity. [1]

2. FEM-PEM Review

2.1 Transmission Loss trim FEM simulation of lightweight automotive dashboard insulators with consideration of the instrument panel

The goal of Dejaeger et. al. was to be able to reduce the mass of an acoustic treatment material behind the instrument panel of a passenger vehicle. Importantly, the focus frequency range was between 250 and 400 Hz. Weight reduction had to be carried out without losing acoustic performance. This meant that the new material had to reduce interior sound levels at least to the degree that its heavier counterpart did. Such an analysis directly involves some modeling of PEM. The authors chose the transfer-matrix method (TMM), which provided them a tool to evaluate the acoustic properties of various material configurations for the sound deadening panel. [2]

By using TMM, the research group was able to eliminate many iterative steps within the full FEA simulation. Only selected material configurations were tested in the full instrument panel simulation, previously proven in the TMM optimization loop. Eventually, a combination of heavy and light layers with localized placement was selected for the final design. On the Figure 1., the bare steel, the original sound insulator, and two proposed insulators (one before, one after the TMM optimization loop) are displayed. It is clear that the optimized design offers great advantages in the focus frequency range, therefore validating the TMM approach for this case.

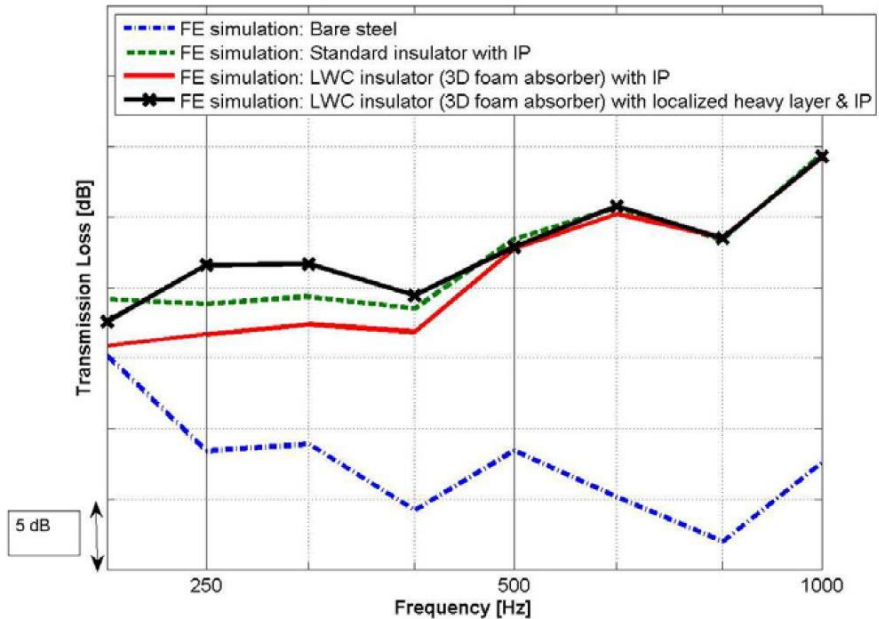


Figure 1.: Transmission loss of four different instrument panel configurations [2]

2.2 Prediction of NVH behaviour of trimmed body components in the frequency range 100-500 Hz

This study, conducted by Cameron and colleagues in Sweden focused on the effects of the headliner on the interior sound levels. As in the previous case, they also opted for modelling the headliner rather than explicitly calculating the Biot-equations for this case. The vehicle chosen was a SAAB 9-3 station wagon, whose roof section was removed. Instead of modelling the three-layer headliner, a homogenous model was used with averaged material properties. This model headliner split the virtual vehicle model's interior cavity into two separate parts: one volume between the roof panel and the headliner, and another volume below the headliner, enclosed by the vehicle body and windows. To validate the simplifications, measurements were conducted on a test rig. [3]

Results of this research campaign are less promising than in the previous one. Data gathered is very noisy, however it is still evident that despite the authors'

claims, there is no good agreement between simulation and measurement (Figure 2).

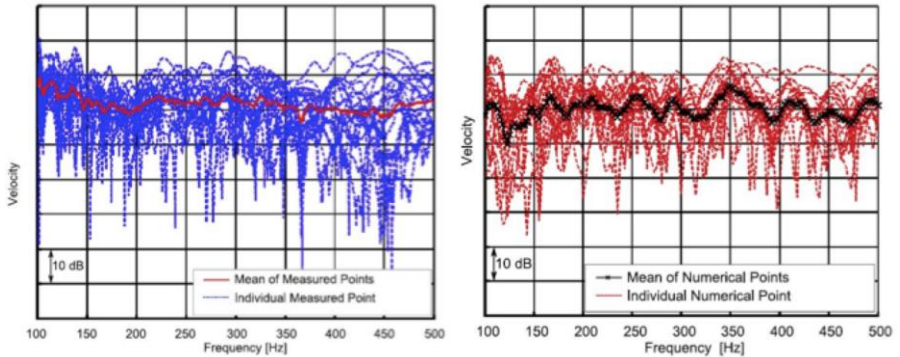


Figure 2.: measured (blue) and calculated (red) results of the headliner [3]

2.3 Dynamic behavior analysis of vehicle acoustic trim using FEM

The goal of the third research team was very similar to that of the first group: reduce simulation time for poroelastic FEA simulations. Similarly, they also manipulated the matrices involved, however, the approach was fundamentally different. Kobayashi and colleagues separated the FEA mesh from the trim element mesh, therefore the FEA and trim meshes were completed by separate algorithms. The two meshes were then solved together in a coupled, self-developed solver. For trim elements, their dynamic stiffness matrix was manipulated, reduced to modal coordinates and then the physical degrees of freedom could also be reduced. This way, simulation time was shortened from over 200 hours to little over 20, which is much more acceptable in an industrial environment. Figure 3 shows that in the lower frequency ranges, simulation and experiment have very good agreement, however from 250 Hz and above, deviation grows from measurement. Still, this method can be considered very successful in applying Biot-theory modelling to a numerical acoustic problem. [4]

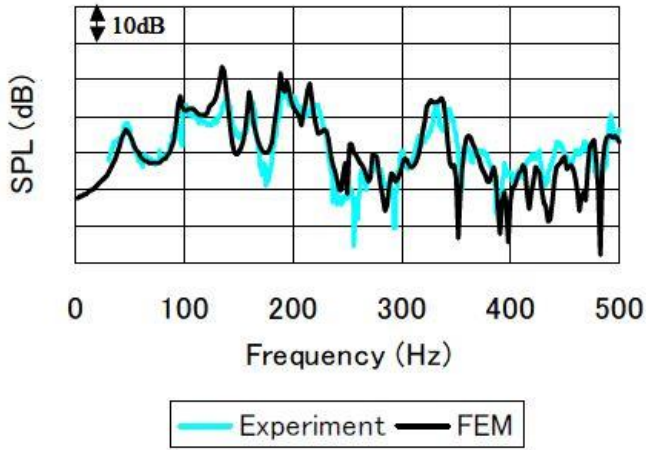


Fig.17 Validation of floor FE model (Absorptive type)

Figure 3.: measurement vs. FEA results of the research [4]

3. Summary

Poroelastic materials are essential to provide adequate passenger comfort in today's cars. To model their effect already in the design phase, Biot-theory is employed during acoustic simulations. Three methods were reviewed to include Biot-theory in industrial calculations, two of whom proved to be quite successful. However, even they were strongly limited in their applicable frequency range, which points researchers to the direction of expanding the frequency regions of such simulations in their future works.

Acknowledgement

The author would like to thank to EFOP-3.6.1-16-2016-00017 'Internationalisation, initiatives to establish a new source of researchers and graduates, and development of knowledge and technological transfer as instruments of intelligent specialisations at Széchenyi István University' for the support of the research.

References

1. Vehovszky, Balázs, „Végeselem módszer – jegyzet”, 2017.

2. Ludovic Dejaeger, Jean-François Rondeau, Patrick Chanudet, Bertrand Auffray. Transmission Loss trim FEM simulation of lightweight automotive dashboard insulators with consideration of the instrument panel. Société Française d'Acoustique. Acoustics 2012, Apr 2012, Nantes, France. 2012.
3. Cameron, Christopher J., et al. "Prediction of NVH Behaviour of Trimmed Body Components in the Frequency Range 100–500Hz." *Applied Acoustics*, vol. 71, no. 8, 2010, pp. 708–721., doi:10.1016/j.apacoust.2010.03.002.
4. Kobayashi, Norimasa, et al. "Dynamic Behavior Analysis of Vehicle Acoustic Trim Using FEM." *The Journal of the Acoustical Society of America*, vol. 123, no. 5, 2008, pp. 3571–3571., doi:10.1121/1.2934644.

Festo prolog factory simulation modelling

N.Szántó

Széchenyi István University, Department of Automobil Production
Technology
H-9026 Győr, Egyetem tér 1. Hungary
szanto@sze.hu

Abstract: This paper contains the description of the simulation modelling of a sample system. The physical system, the process simulation tool and the simulation steps are presented. The purpose of modeling is to analyze the digital twin of the system based on predefined boundary conditions.

Keywords: prolog factory, process simulation, digital twin

1. Introduction

The simulation modelling of the sample system is designed to assist in phases of data collection, data analysis, forward planning and virtual extensions. Another objective of the completed model is to create a digital twin for the sample system. From the point of view of the system, the creation of a digital twin has several conditions, in this article only the creation of a simulation model is presented.

2. Description of the physical system

The precondition for preparing the simulation model is to know the structure, components and their relationships, operating conditions, communication and control of the existing resource. At the sample production line, there are nine modular cells (Figure 1) where three types of products can be manufactured. Each cell has a separate PLC control, through sensors and actuators a linear flow is realized between the stations.

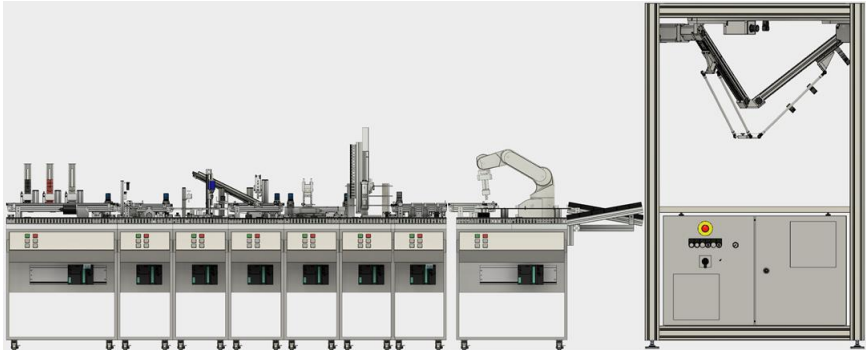


Figure 1. Festo prolog factory front view

Workpieces can be ordered and started via WINCC. The line are feeded by the first station (triple stack magazine station) with the ordered products and to the storing station (station 6th) workpieces flow station to station. After ordering, the workpiece is delivered to the order-picking station from the storing station. Workpieces going through the manufacturing process fill the shortage caused by ordered goods removed from the warehouse. Workpieces received at the picking station should be placed on a palette according to a specific layout, the palette having four (2x2) capacities, 1-4 workpieces can be loaded. In the last step, the palette is moved to a tripod by a robot.

3. System definition of the simulation model

The applied software is Tecnomatix Plant Simulation developed by Siemens. Plant Simulation provides discrete event simulation and statistical analysis capabilities with object-oriented environments to model, simulate and optimize manufacturing systems and their processes. The realization of a simulation model based on a real system consists of the following four main steps:

1. Preparation: problem definition, target definition, system definition, requirements, data collection
2. Modelling: model building, model validation
3. Experimentation: simulation pilot design, simulation runs, performance evaluation, system optimization.
4. Implementation: practical application of simulation results, documentation.

The process is iterative, and each process step can affect the previous process (feedback option).

First, the system to be simulated needs to be understood in general. From the goal definition, the degree of detail of the simulation needs to be decided and based on the expected accuracy of the decision, which decisions need to be simplified or not taken into account at all. With the completed model (Figure 2) experiments can be performed, the results can be evaluated and interpreted in the real system.

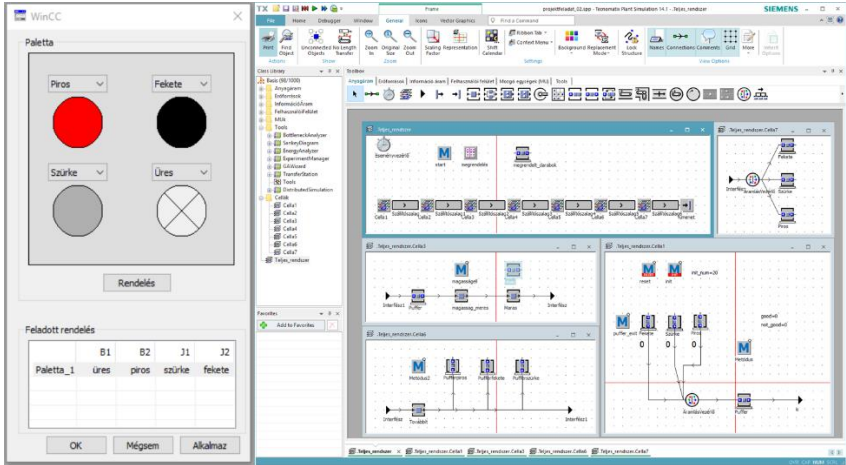


Figure 2. Simulation view

The parts of the sample system cells were modelled separately by the detailed implementation of the current control structure. Consistent behaviour of cells, deployment, active-inactive jobs, work order, virtual workplaces are controlled by a higher control in the simulation.

4. Summary

With the presented model data collection and data analysis can be more efficient. The model also creates the preconditions for creating a digital twin, in which the simulation model's behavior is determined by real-time data from the real system.

Acknowledgement

The authors would like to thank to EFOP-3.6.1-16-2016-00017 'Internationalisation, initiatives to establish a new source of researchers and graduates, and development of knowledge and technological transfer as instruments of intelligent specialisations at Széchenyi István University' for the support of the research.

References

1. W. Kühn, Digitale Fabrik: Fabriksimulation für Produktionsplaner, Hanser, München, 2006.
2. Schober, Manual prolog-factory, Festo Didactic GmbH & Co.KG, Denkendorf, 2010
3. S. Bangsow, Tecnomatix Plant Simulation, Springer, 2015

Numerical examination of simple nonlinear systems

F. Hajdu

**Széchenyi István University, Faculty of Mechanical Engineering, Informatics and Electrical Engineering, Department of Mechatronics and Machine Design
Egyetem tér 1., 9026 Győr, Hungary
e-mail: hajdfi@sze.hu**

Abstract: This paper presents the numerical examination of different nonlinear systems. 3 simple nonlinear systems, a nonlinear electrical circuit, the unforced Van der Pol oscillator and the Duffing-Holmes oscillator were examined with time diagrams, phase-plane diagrams, Poincaré sections and frequency diagrams. It was observed how the change in certain parameters affects the behaviour of the systems.

Keywords: *numerical analysis, nonlinear system modeling, Maple*

1. Introduction

Similarly to linear systems nonlinear systems can be examined in the time domain and in the frequency domain with different numerical methods.

Besides time diagrams one of the most effective methods to study nonlinear systems in the time domain is the numerical creation of phase-plane diagram, which shows 2 state variables and their trajectories 1.

The bifurcation diagram shows the change in the topology of the system as the bifurcation parameter is varied, e.g. the change in equilibria points and periodic orbits 2. To study the effects of changing 2 parameters at the same time a 2 parametric bifurcation diagram can be constructed 3.

For complex nonlinear systems sometimes the phase-plane diagram can be difficult to study. To simplify the examination we can create the Poincaré section, which is the cross-section of a trajectory with a plane in the state-space 4.

In the frequency domain besides frequency response diagrams 3D frequency spectrum maps can be created which represent the change of frequency components, when a parameter varied 5.

A more detailed description of the numerical construction of the mentioned diagrams is described in 6. Other examination methods of nonlinear systems are presented in 7.

In this paper the use of the mentioned numerical examination methods on simple nonlinear systems is presented.

2. Numerical examination of simple nonlinear systems

In this section 3 different simple nonlinear systems are studied with numerical methods: a nonlinear electrical circuit, the unforced Van der Pol oscillator and the Duffing-Holmes oscillator⁸.

2.1 A nonlinear electrical circuit

An electrical circuit with a nonlinear Tunnel diode was examined. The differential equation of the system is:

$$\dot{x}_1 = \frac{1}{C} [-h(x_1) + x_2] \tag{1}$$

$$\dot{x}_2 = \frac{1}{L} [-x_1 + Rx_2 + E] \tag{2}$$

The phase-plane diagram, and the bifurcation diagrams of the circuit can be seen in *Fig. 1*.

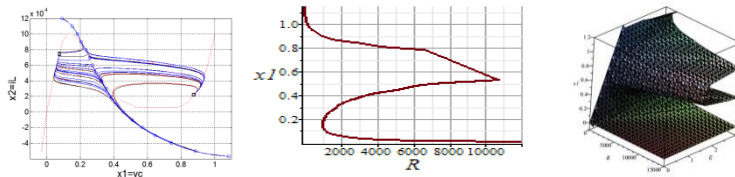


Fig. 1.: The phase-plane diagram at the boundary line of sets of attraction (left), the bifurcation diagram of the resistance (middle) and the 2 parametric bifurcation diagram (right) of a nonlinear Tunnel diode circuit⁹

From the phase-plane diagram besides the trajectories from different states the boundary line of sets of attraction can be observed. From the bifurcation diagrams the number of equilibria points can be seen: there are parameter values when there is 1, 2 or 3 equilibria points. This information can be useful for example to design a switching circuit. A more detailed examination of this electrical system can be found in 9-10.

2.2 The unforced Van der Pol oscillator

The Van der Pol oscillator is a simple nonlinear oscillator. The numerical examination of it is very useful as it can be used to model more difficult nonlinear phenomena [11-12]. The differential equation of the unforced oscillator is:

$$\frac{d^2}{dt^2} x(t) = \mu(1 - x(t)^2) \frac{d}{dt} x(t) - x(t) \quad (3)$$

The phase-plane diagrams for different μ parameters can be seen in Fig. 2.

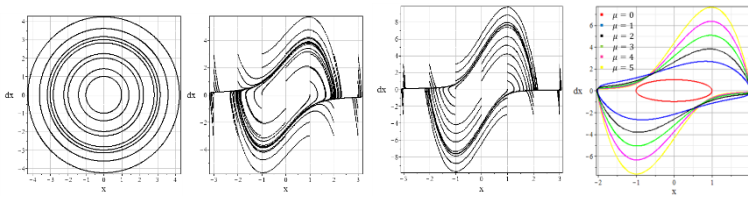


Fig. 2.: Phase-plane diagram of the Van der Pol oscillator ($\mu=0$, $\mu=2$, $\mu=5$ and the limit cycle as μ is varied from 0 to 5)

In case of $\mu=0$ it is a simple linear oscillator, therefore there is a circle on the phase-plane diagram for every initial condition. If $\mu>0$ a limit cycle exists. Changing parameter μ changes the limit cycle, as it can be seen in Fig. 2 right. The time diagrams of x and dx and the frequency response diagram for x can be seen in Fig. 3. The initial conditions were $x(0)=1$ and $dx(0)=0$ in all cases.

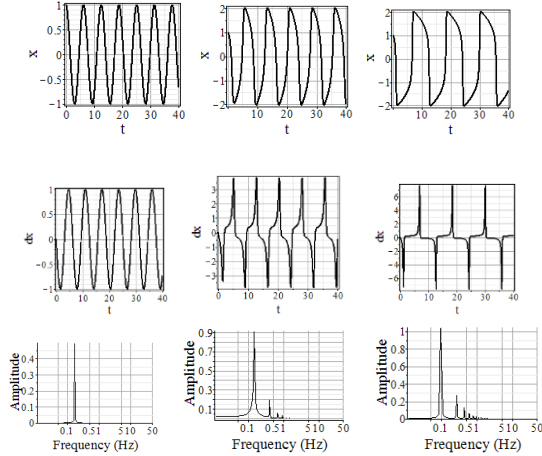


Fig. 3.: x -time diagram (up), dx -time diagram (middle) and frequency response diagram (down) of the Van der Pol oscillator ($\mu=0$, $\mu=2$ and $\mu=5$)

It can be seen that if $\mu=0$ a harmonic periodic oscillation occurs, therefore there is only one frequency component. In the case of $\mu>0$ a relaxation oscillation occurs. The period time increases as parameter μ is increased

2.3 Duffing-Holmes oscillator

The Duffing-Holmes oscillator is a well-known simple nonlinear system. It can be used for example to model chaotic behaviour of a vehicle suspension system 13. The equation system is:

$$\frac{d^2}{dt^2}x(t) + \delta \frac{d}{dt}x(t) + \alpha x(t) + \beta x(t)^3 = \gamma \cos(\omega t) \quad (4)$$

From the differential equation it can be seen that there are several system parameters. In this study parameters $\alpha=1$, $\beta=1$, $\delta=0.15$ and $\omega=1$ were chosen as constants and parameter γ was varied. In all test cases $x(0)=1$ and $dx(0)=0$. The bifurcation diagram can be seen in Fig. 4

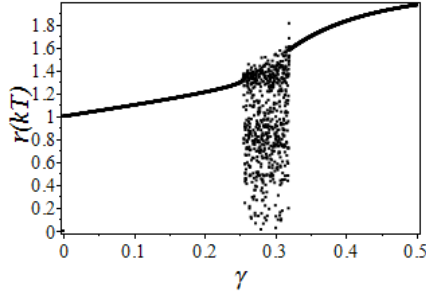


Fig. 4.: Bifurcation diagram of the Duffing-Holmes oscillator

It can be seen that when $\gamma < 0.25$ or $0.32 < \gamma$ there is a harmonic oscillation or a stable limit cycle, when $0.25 < \gamma < 0.32$ chaotic oscillation occurs.

In *Fig. 5* several test results can be seen. It can be seen if $\gamma = 0.1$ a harmonic oscillation occurs, so there is only a single point at the Poincaré section and one frequency component. A circle can be seen at the phase-plane diagram, which is also a sign of harmonic oscillations. If $\gamma = 0.25$ there is a subharmonic oscillation and therefore at the Poincaré section as there are 3 points. At the frequency-response diagram it can be seen that there are 2 main frequency components. If $\gamma = 0.3$ chaotic oscillation occurs, a chaotic attractor can be seen at the Poincaré section. At the frequency response diagram it can be seen that there are several components, which is also a sign of chaotic behaviour. If $\gamma = 0.4$ a mildly subharmonic oscillation occurs with a stable limit cycle. At the Poincaré section there is only a single point and at the frequency response diagram there is a main frequency component and another component with small amplitude.

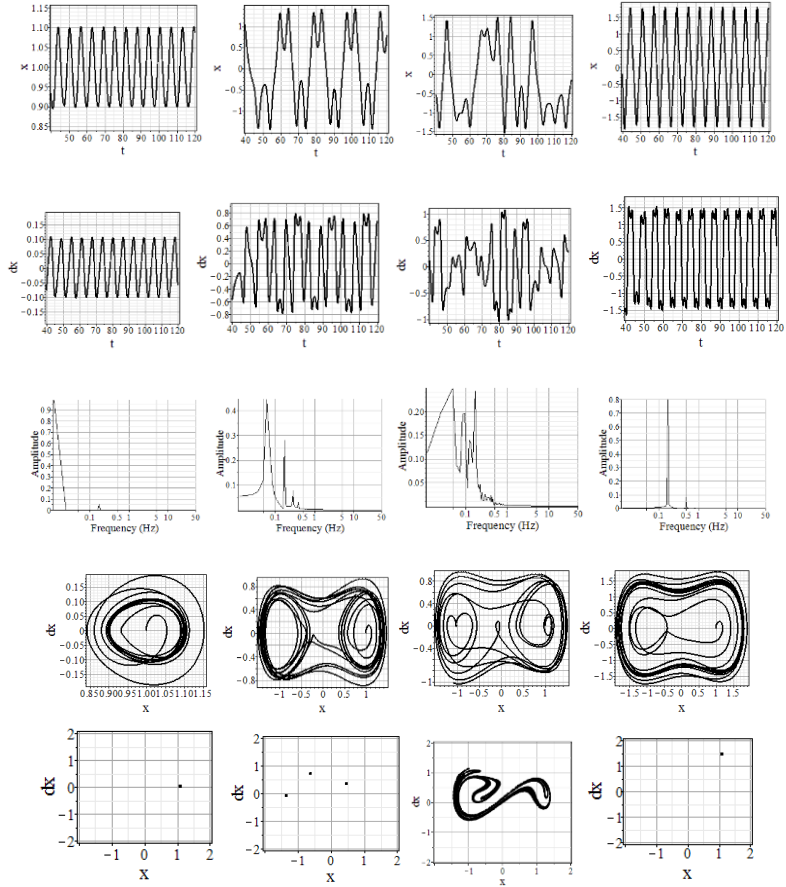


Fig. 5.: Time diagrams, frequency diagrams, phase-plane diagrams and Poincaré sections of the forced Van der Pol oscillator ($\gamma=0.1$, $\gamma=0.25$, $\gamma=0.3$ and $\gamma=0.4$)

3. Conclusions

The numerical examination of 3 simple nonlinear systems was carried out with numerical methods. It was observed how different parameters affect the system's behaviour. In case of a simple bistable electrical system the change in the resistance results in change in the number of equilibria points. In case of the unforced Van der Pol oscillator the change in parameter μ results in the change in the limit cycle. In case of the forces Van der Pol oscillator the change in parameter

γ results in the change in the system's behaviour: there are cases when there is harmonic, subharmonic and chaotic oscillation.

Acknowledgement

The author would like to thank to EFOP-3.6.1-16-2016-0001 'Internationalisation, initiatives to establish a new source of researchers and graduates, and development of knowledge and technological transfer as instruments of intelligent specialisations at Széchenyi István University' for the support of the research.

References

1. P. Simon: Differential Equations and Dynamical Systems (in Hungarian). Eötvös Loránd University, lecture notes, Budapest, Hungary, 2013 [cited 2016.06.22.], http://www.tankonyvtar.hu/hu/tartalom/tamop412A/2011_0025_mat_11/index.html
2. Y.A. Kuznetsov: Elements of applied bifurcation theory, Springer, 1998.
3. F. Hajdu: Parallel numerical creation of 2-parametric bifurcation diagram of nonlinear oscillators, Acta Technica Jaurinensis (accepted)
4. B. Garay: Nonlinear Dynamical Systems (in Hungarian), Pázmány Péter Catholic University, lecture notes, Budapest, Hungary, 2013 [cited 2018.06.22] http://www.tankonyvtar.hu/en/tartalom/tamop412A/2011-0052_20_nemlinearis_dinamikus_rendszerek/index.html
5. S.A. Billings, O.M. Boaghe: The response spectrum map, a frequency domain equivalent to the bifurcation diagram, *International Journal of Bifurcation and Chaos*, July 2001, Vol. 11, No. 07, 2001 pp. 1961-1975
6. F. Hajdu: Numerical Examination of Nonlinear Oscillators, Pollack Periodica (accepted)
7. L.A. Aguierre: A Tutorial Introduction to Nonlinear Dynamics and Chaos, Part 1: Tools and Benchmarks, SBA Controle & Automacao, Vol. 7 No. 1, 1996, pp. 29-49
8. H.K. Khalil: Nonlinear Systems, Prentice Hall, 1999
9. F. Hajdu, Gy. Molnárka: Numerical examination of a system model with a nonlinear component, Proceedings of the 8th International Scientific and Expert Conference, Trnava, Slovakia, 19-21 October 2016, pp. 12–16.

10. F. Hajdu: Numerical examination of a nonlinear circuit element (in Hungarian), Proceedings of the 5th Interdisciplinary Doctoral Conference *Conference*, Pécs, Hungary, 27-29 May 2016, pp. 142–154.
11. D.H. Peluffo-Ordonez, J.L. Rodríguez-Sotelo, E.J. Revelo-Fuelagán, C. Ospina-Aguirre, G. Olivard-Tost: Generalized Bonhoeffer-van der Pol oscillator for modelling cardiac pulse: Preliminary results, 2015 IEEE 2nd Colombian Conference on Automatic Control (CCAC), 2015,
12. M.L. Facchinetti, E. Langre, F. Biolley: Vortex shedding modeling using diffusive van der Pol oscillators, *Comptes Rendus Mécanique*, Vol. 330, No 7., 2002, pp. 451-456
13. G. Litak, M. Borowiec, M. I. Friswell, K. Szabelski: Chaotic vibration of a quarter-car model excited by the road surface profile. *Communications in Nonlinear Science and Numerical Simulation*, Vol. 13 No.7, 2008, pp. 1373-1383

HDPE/PA hybrid nanocomposites

H. Hargitai¹, N. Bíró²

^{1,2} Széchenyi István University, Department of Materials
Science and Technology
Egyetem square 1, 9026 Győr, Hungary
e-mail: hargitai@sze.hu

Abstract: HDPE/PA6 micro-nanocomposite blends containing glass fiber and glass bead were produced by laboratory twin screw extruder. Mechanical properties, processability and microstructure of these blends were examined. The effect of adding different proportions of coupling agent (PE-g-MA) and organoclay (montmorillonite) were also studied. Based on the scientific literature it was expected the organoclays going to result smoother structure of these blends which comes with better mechanical properties and heat resistance features. It was supposed that the chemical coupling agent provides better interaction between the phases.

Keywords: polymer blend, nanocomposite, montmorillonite, glass fibre

1. Introduction

Polymer blends are widely applied to tailor materials for specific applications. PA6 and HDPE blends combine thermomechanical characteristics of the former with the ease of processing of the latter [1, 2]. Significant numbers of polymer blends are immiscible and incompatible, and thus a phase separations occurred which has a great influence on the mechanical properties [3, 4]. The blend morphology and the adhesion on the interfaces can be influenced by several methods. Using compatibilizing agents as maleated polyethylene or organic nanoclays can reduce the interfacial tension and may resulted in dramatic improvements in mechanical, thermal and barrier properties [5, 6]. Nanoparticles have strong effect on the microstructure of the immiscible polymer blends; they resulted in the decrease of the minor phase and thus finer microstructure [7-10].

Clifford and Wan showed that there is synergy in combining disparate reinforcements; the weight saving is achieved by including clay in glass fibre composites, which enhances and allows the higher modulus of materials to be manufactured [11].

In our experiments immiscible polymer blends composed of HDPE and PA6 containing glass bead and glass fibre were produced, montmorillonite and chemical coupling agent in different amounts were added and their effect on the mechanical properties and the microstructure were analysed.

2. Experimental

2.1 Materials

All the materials used in this study are commercially available. High-density polyethylene (HDPE, TIPELIN 6000B (TVK, Hungary), MFR: 1.30 g/10 min (5 kg, 190 °C), and reinforced polyamide 6 (PA6-(GF10+GB20), Ultramid B3GK24) were blended as matrix materials. Chemical coupling agent (Polybond 3009 (Chemtura Corp.) – PEGMA (Mw=186000)) was added in 1wt% (related to the matrix weight) – to the polymer blends. As nano reinforcement layered structure montmorillonite (MMT, Cloisite 20 A, Southern Clay Products) was applied.

2.2 Sample preparation

Sample preparation was a two-step process, proposed from compounding by a laboratory twin screw extruder (210 to 260°C) and test specimen preparation by injection moulding. In the melt mixing step PEGMA (1% and 3%) and MMT (1% and 3%) were incorporated separately or in a combination of 1% PEGMA and 3% MMT. Amounts of PEGMA and MMT are related to the common weight of HDPE and reinforced PA6. The raw materials were dried before the extrusion and the injection moulding at least 4 hours on 80°C.

2.3 Testing methods

The specimens used for three point bending and the impact tests were made by cutting the ends of the dumb-bell shaped samples. All specimens were conditioned (50% RH, 23°C) at least 24 hours before testing. Mechanical properties were determined by tensile test, three point bending tests and Charpy impact test. The morphology of the blends was characterized by scanning electron microscope (SEM).

3. Summary of results

Based on the results of the mechanical tests and microscopic investigations the main results are introduced as the following.

Applying of 1% and 3% PE-g-MA increased the tensile strength of blends. The greatest improvement (15%) could have been reached by adding 3% coupling

agent to the blend, while the maximum improvement in Young's modulus was found by adding 3% MMT (Figure 1).

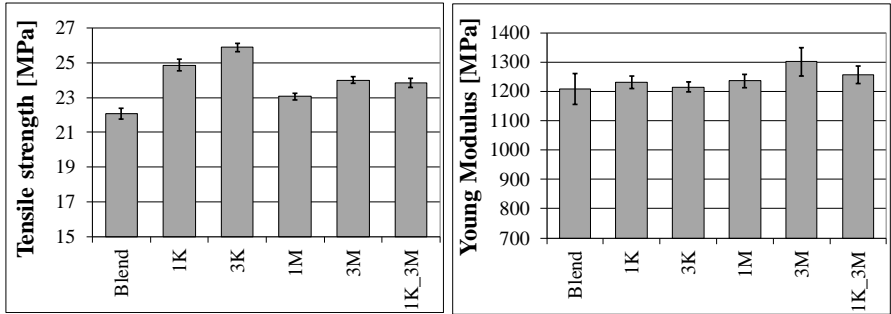


Figure 1. Tensile strength and Young's modulus of blend and the hybrid composites (K: PEGMA, M: MMT)

By using 3% MMT a slight increase was found in the case of three point bending properties. As a result of scanning electron microscopy investigations, it was found that both PE-g-MA and MMT result in a refinement of the structure, significantly reducing the size of the precipitated phases. This effect is particularly pronounced when both PE-g-MA and MMT are added (Figure 2).

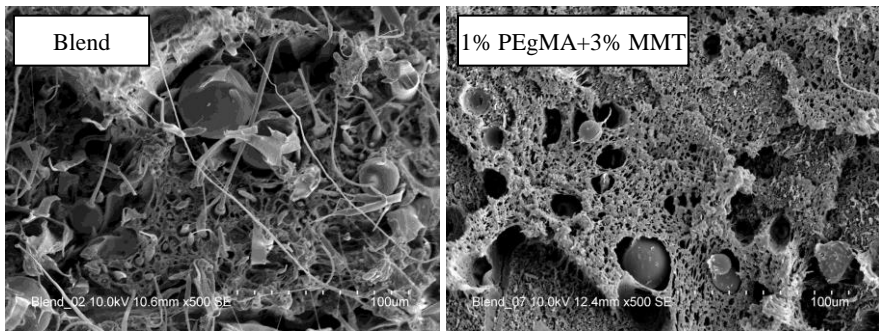


Figure 2. SEM micrograph of the fractured surface of the pure blend and the composite with 1% PEGMA and 3%MMT

Acknowledgement

The authors would like to thank to EFOP-3.6.1-16-2016-00017 'Internationalisation, initiatives to establish a new source of researchers and graduates, and development of knowledge and technological transfer as

instruments of intelligent specialisations at Széchenyi István University' for the support of the research.

References

1. H. Hargitai, I. Rácz, Applications of Macro- and Microfiller-Reinforced Polymer Composites in Polymer Composites: Volume 1, Wiley-VCH Verlag GmbH & Co. KGaA, 2012, pp. 749-79.
doi: 10.1002/9783527645213.ch23
2. L.A. Utracki, Commercial polymer blends, Chapman and Hall, London 1998.
doi: 10.1002/(SICI)1097-0126(200004)49:4<417::AID-PI355>3.0.CO;2-I.
3. H. Pernot, M. Baumert, F. Court, L. Leibler, Design and properties of co-continuous nanostructured polymers by reactive blending, Nature Materials 1 (2002) pp. 54–58.
doi: 10.1038/nmat711
4. G. Filippone, N.Tz. Dintcheva, F.P. La Mantia, D. Aciern, Using organoclay to promote morphology refinement and co-continuity in high-density polyethylene/polyamide 6 blends - Effect of filler content and polymer matrix composition, Polymer 51 (2010) pp. 3956-3965.
doi: 10.1016/j.polymer.2010.06.044
5. W.-T. He, S.-T. Liao, Y.-S Xiang, L.-J Long, S.-H Qin, J. Yu, Structure and properties study of PA6 nanocomposites flame retarded by aluminium salt of diisobutylphosphinic acid and different organic montmorillonites, Polymers 10 (2018) p. 312.
doi:10.3390/polym10030312
6. Ahmad Nawaz Khan, Bilal Anjum, Comparative study of polyamide6 reinforced with glass fibre and montmorillonite, Polymer Bulletin 72 (5) (2015) pp. 1207-1216.
doi: 10.1007/s00289-015-1333-4
7. W. S. Chow, Z. A. Mohd Ishak, J. Karger-Kocsis, Morphological and rheological properties of polyamide 6 / poly(propylene) / organoclay nanocomposites, Macromolecular Materials and Engineering 290 (2005) pp. 122-127.
doi: 10.1002/mame.200400269
8. M. H. Lee, C. H. Dan, J. H. Kim, J. Cha, S. Kim, Y. Hwang, C. H. Lee, Effect of clay on the morphology and properties of PMMA/poly(styrene-co-acrylonitrile) / clay nanocomposites prepared by melt mixing, Polymer 47

- (2006) pp. 4359-4369.
doi: 10.1016/j.polymer.2006.04.003
9. S. Mallick, B. B. Khatua, Morphology and properties of nylon6 and high density polyethylene blends in absence and presence of nanoclay, *Journal of Applied Polymer Science* 121 (2011) pp. 359-368.
doi: 10.1002/app.33580
 10. H. Hargitai, T. Ibriksz T, J. Stifter, E. Andersen, Development of PA6/HDPE nanocomposite, *Materials Science Forum* 729 (2013) pp. 216-221.
doi: 10.4028/www.scientific.net/MSF.729.216
 11. Mike J. Clifford, Tong Wan, Fibre reinforced nanocomposites: Mechanical properties of PA6/clay and glass fibre/PA6/clay nanocomposites, *Polymer* 51 (2) (2010) pp 535-539.
doi: 10.1016/j.polymer.2009.11.046.

Influence of DMLS parts building orientation on the part surface roughness

I. Hatos

Széchenyi István University, Department of Materials Science and Technology
Egyetem square 1, H-9026 Győr, Hungary
e-mail: hatos@sze.hu

Abstract: The build orientation has a large effect on the printed part quality and building time. The determination of building orientation and support structures probably the most important engineering task during the production process. The relatively poor surface quality and overhanging surface fabrication still presents a major limitation in the metal 3D printing process. In this study an investigation of surface roughness presents for parts made by DMLS at different sloping angles.

Keywords: *DMLS, 3D printing, building orientation, surface roughness*

1. Introduction

Selective laser sintering (SLS) belongs to the rapid prototyping (RP) technologies. In SLS systems, a 3D part is built by melting thin layers of powdered thermoplastic materials or metals layer-by-layer, using a laser beam. DMLS (Direct Metal Laser Sintering) means laser sintering parts from metal powders, without binders. By producing the part layer by layer from metal powder extremely complex metal parts can be made. Some special sectors using mainly this technology: medical, aerospace and automotive. A promising field of the applications of DMLS is polymer tooling by producing mold insert for injection molding with special cooling systems (conformal cooling) **Hiba! A hivatkozási forrás nem található.Hiba! A hivatkozási forrás nem található..**

One of the critical choices during production is the selection of the build orientation. As the build orientation has a large impact on the final part quality, it must be chosen wisely. DMLS process requires external support structures. The support structures increases both the time required for the layer manufacturing and the time of post-processing operations. Minimizing the amount of supported surfaces can improve the process efficiency. The design and optimization of the support structures are necessary to improve the sustainability and efficiency of metallic parts produced by DMLS. Depending of the object built orientation, the

surface area of support structure change sensitively. There are engineering softwares for the automatic and manual generation of structure supports such as that developed by Materialise Company, Magics 4.

The purpose of this research is to understand the relationship between the surface roughness and building orientation.

2. Experimental

For the experiments MS1 maraging steel (1.2709) powder from EOS widely used in DMLS systems (see Table 1.) were used.

Table 1. Chemical compositions of maraging steel tool materials

<i>Material</i>	<i>C</i>	<i>Cr</i>	<i>Ni</i>	<i>Mn</i>	<i>Si</i>	<i>Al</i>	<i>Co</i>	<i>Mo</i>	<i>Ti</i>
MS1	<0.03	<0.5	17-19	<0.1	<0.1	0.05-0.15	8.5-9.5	4.5-5.2	0.6-0.8

Experiments were performed on the EOS M270 at SZE ATT. The powder used for the specimens was powder reclaimed from prior jobs using an 80 μm sieve.



Figure 1. MS1 powder

To investigate the impact of different building orientation on the surface quality of the printed part, simple cuboids with different angles were analyzed. The specimens were designed as parallelepipeds with varying angles of overhang (α) to determine the effect of overhang angle on the surface roughness of the downward- and upward-facing surface (Figure 2.). To analyze a wide range of different angles measured from the building platform, a range between 0° and 90° is chosen. Prior experience has shown that the 0° - 30° overhang would build poorly without supporting structures.

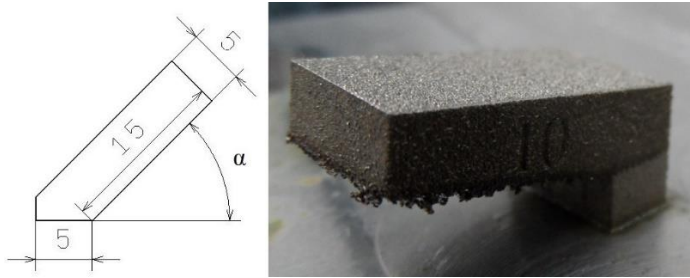


Figure 2. 2D drawing about the specimen (left) and $\alpha=10^\circ$ printed part (right)

3. Results

Analysis of Ra values can be seen in Figure 3., which shows a dependence of α angle on Ra. The results show that an angle around 10° increase the roughness drastically in case of upward-facing. The best Ra values measured between 60° and 90° for both face. Not self-supporting surfaces are surfaces which are downward oriented and α angle is less than 50° degrees with respect to platform.

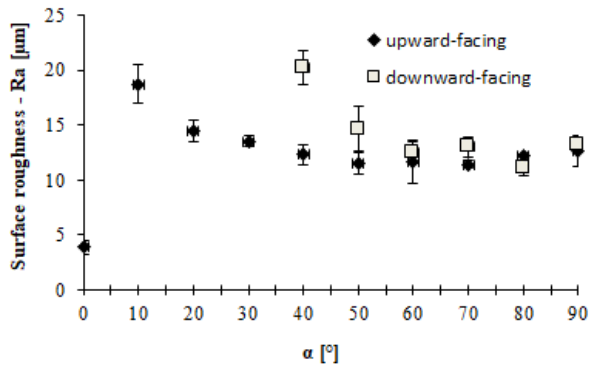


Figure 3. Surface roughness versus α angle

Acknowledgement

The authors would like to thank to EFOP-3.6.1-16-2016-00017 'Internationalisation, initiatives to establish a new source of researchers and graduates, and development of knowledge and technological transfer as instruments of intelligent specialisations at Széchenyi István University' for the support of the research.

References

1. S. A. M. Tofail, E. P. Koumoulos, A. Bandyopadhyay, S. Bose, L. O'Donoghue, C. Charitidis, Additive manufacturing: scientific and technological challenges, market uptake and opportunities, *Materials Today* 21 (1) (2018) pp. 22-37
<https://doi.org/10.1016/j.mattod.2017.07.001>
2. Hatos, H. Hargitai, L. Solecki, Study of 2D and 3D methods for worn surface analysis of tool materials, *Acta Technica Jaurinensis*, 8 (2) (2015) pp. 165-178, 2
<https://doi.org/10.14513/actatechjaur.v8.n2.373>
3. M. P. Zwier, W. W. Wits, Design for additive manufacturing: Automated build orientation selection and optimization, *Procedia CIRP* 55 (2016) pp. 128-133
<https://doi.org/10.1016/j.procir.2016.08.040>
4. F. Calignano, D. Manfredi: Production of overhanging structures by DMLS, The International Conference on Advanced Research in Virtual and Rapid Prototyping (VRAP), Leira, Portugal (2016)

Condition Monitoring Method Development for Electric Motor Bearings with Vibration Analysis and Accelerated Aging Process

M. Pesthy¹ – Cs. Tóth-Nagy¹ – O. J. Richarz² – B. B. Tóth²

¹Széchenyi István University, Audi Hungaria Faculty of Automotive Engineering, Department of Internal Combustion Engines, H 9026 Győr, Egyetem Tér 1., Tel.: +36 70/883-4180, e-mail: mark.pesthy@gmail.com

²Audi Hungaria Zrt., H 9027 Győr, Audi Hungária u. 1., G/GE-4

Abstract: Due to the ever increasing expectations toward internal combustion engines during the dynamometer testing, the development of the measuring equipment is a particularly important topic. It can result in significant cost and time savings if the dynamometer - as the most important component - does not cause unexpected time out due to its mechanical failures (eg. bearing). Furthermore, the avoidance of consequent failures on the test engine being tested is also important. A research project was carried out to accelerate the aging of electric machine bearings electrically, while bearing condition was monitored with an accelerometer. The article presents the aging process and the developed measuring method, and discusses the results.

Keywords: condition monitoring systems, accelerometer, structure-borne noise testing, bearing, accelerated aging

1. Introduction

During the testing of automotive engines, it is essential that the testing dynamometers to operate at 100% safety. This paper focuses on the bearings of the dynamometers electric machine's. Bearings are the wearing components of an electric machine. Bearings may fail and it may result in minor or major damages to other components, even the engine performing on the test. After such a bearing failure, the experiments are often forced to shut down that results in an increase in testing time, resulting delays and increased costs in production.

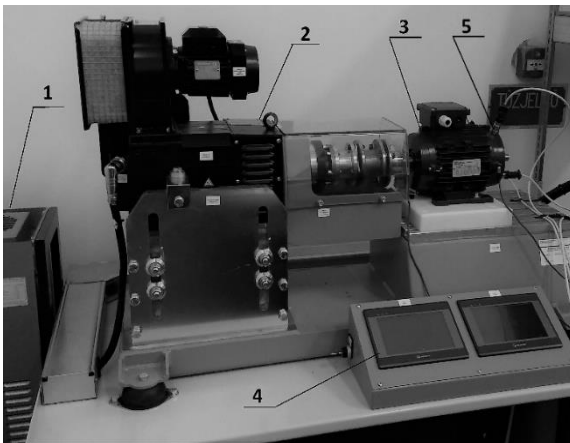
In order to avoid delays, it is important to predict the possible failures and the condition of the bearings. For a bearing that can be operated over ten thousands of operation hours, detailed mapping of its entire service life will take a long time.

The accelerated aging process offers an alternative to this, so that the wear process can be fully modelled, as the failure occurs within 1-2 hours – depending on the load parameters [1][2][3].

2. Experimental Equipment

The experiments were carried out on an electric motor test bench (Figure 1). The system consisted of an asynchronous motor as a dynamometer (5.5 kW) providing the load and an experimental motor (1.5 kW) that held the investigated bearing. The dynamometer was able to measure torque and speed during the tests.

For accelerating the experiments, the tested bearing was aged with steady load, in this case electrically. For the bearing aging, a 30 V alternating voltage has been connected to the housing and the shaft of the electric motor (through carbon brush), which accelerated the aging and the failure of the bearing during the operation of the electric motor.



1. Frequency inverter of the loading motor
2. Loading motor
3. Test motor
4. User interface
5. Accelerometer
6. Torque sensor

Figure 1: The experimental equipment was an electric motor dynamometer

Prior to the aging process, the electrical isolation of the following components was ensured in order to avoid further damage to the equipment:

- Shaft of the tested motor: using plastic bushings – electrically insulated in the direction of the coupling between the two motors. (Figure 2, Component 1)

- The rear bearing has been aged from the direction of the drive shaft and the front one is an insulated ceramic ball bearing. (Figure 2, Component 2)
- Insulated baseplate was placed between the tested motor and the test bench pedestal. (Figure 2, Component 3)

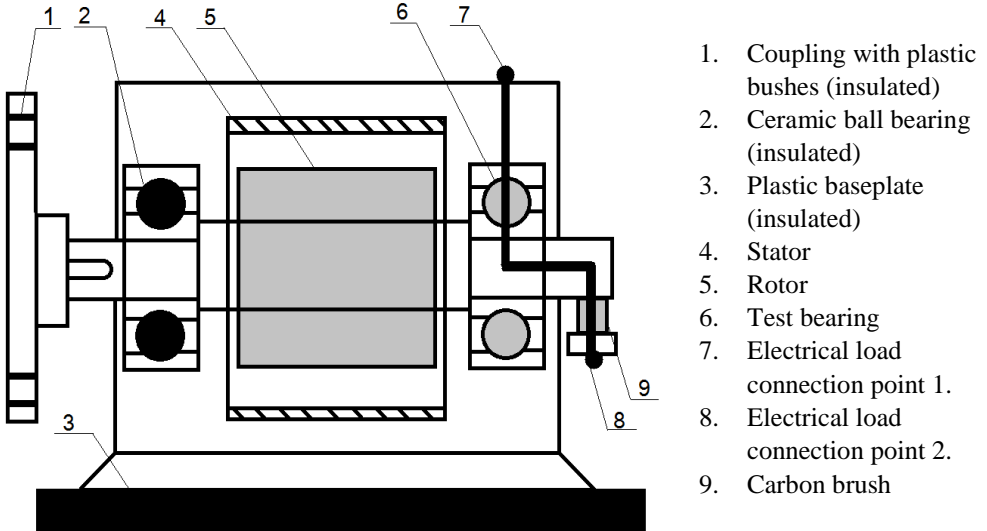


Figure 2: Additional components for the aging process

3. Method of Accelerated Aging

Seker and Dikun presented an electrical aging method, where the electrical aging was performed and seven times repeated, in 30 minutes long cycles, alternating voltage was used [4][5]. The current must flow through the bearing when one of the voltage sources is attached to the housing of the electric motor, which is also the bearing housing, and the other voltage source through a carbon brush to the shaft of the motor. With 1500 RPM, and with 30 V alternating voltage was the electrical load performed. Most of the bearing failures could be detected in 1.25-1.5 hours, so the planned state of the seven planned cycles was already available with three applications. The process was carried out on four standard 6205 serial number bearings without a grease and sealing.

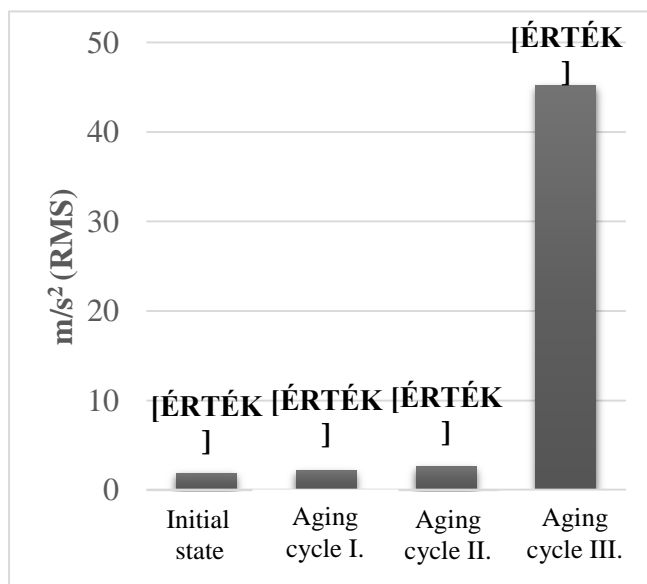
4. Measurement and Data Acquisition

Measurements were made with a device, called SQuadriga II, from HEAD acoustic. The device received three unidirectional analogue ICP accelerometer, which were glued to the housing of the electrical motor and recorded at 24 kHz sample rate. The recordings were manually made on stable working points at two different speeds (600, 1500 RPM), about 15-18 seconds long, and more randomly selected four-second intervals were averaged. Each recording was evaluated but in this study only significant changes are shown. Therefore, the signal from the three directions (axial, vertical and horizontal) of the vertical sensor alone provided sufficient information on the condition of the bearing.

5. Measurement Results

The raw signal perceived by the vertical acceleration sensor was evaluated in several states by several methods, but because of its reliability it was quantified with a root mean square value (RMS), calculated from the signal in the given state (Figure 3).

From the RMS values without further calculations it can be stated that the moment of damage occurred sometime in the 3rd cycle, and it was 1-1.5 minutes long based on observations, while the silent bearing sound became continuous bearing noise.



3. Figure: RMS values for three aging cycles

A summary table was created about the measured and evaluated results. The 1. table shows:

- the root mean square from the raw signal, which is a statistical measure for identifying continuously variable acceleration values
- the absolute value of the peak value of the recording
 - the crest factor, which is the ratio of the peak value and the RMS, which is an unmatched quantity, focusing it is important because its value can increase dramatically in case of bearing wear [3].
- the peakness or kurtosis, which shows the slope of the distribution curve in the context of the modus, so it can be useful to identify the transients in the raw signal and the spontaneous deformations that are important to consider during the bearing test, its calculation method:

$$\text{Kurt} [X]=E\left[\left(\frac{X-\mu}{\sigma}\right)^4\right] \quad (1.)$$

Table 1. fully collaborates the facts set out in Figure 3, that also means, the failure in the third aging cycle can be illustrated by all the calculation methods. The result can be misleading in the case of crest factor and kurtosis, which can be explained by the environmental impact of the calculation method – especially at lower speeds. The applicability of the RMS based limit value monitoring, on the other hand, with the help of simpler calculations was undoubtedly proven.

Different calculated quantities of the three aging cycles – 1. Table

	Root Mean Square (RMS)		Peak value		Peak/RMS (Crest Faktor)		Kurtosis	
	600	1500	600	1500	600	1500	600	1500
RPM Initial state	0,3208	1,8935	1,545	4,3425	4,8169	3,5991	3,172	2,7934
Aging cycle I.	0,6343	2,1813	3,1586	8,6175	4,9791	3,9505	3,0901	2,9897
Aging cycle II.	1,0155	2,5989	4,5796	9,802	4,5093	3,7715	4,0498	2,7658
Aging cycle III.	7,7944	45,1581	40,3708	209,0061	5,1794	4,6283	3,9867	3,1091

6. Conclusion

This paper focused on the accelerated aging process of ball bearings and demonstrated the aging properties of the electrical machine's bearings by using accelerometers mounted on the electric machine's housing.

The usability of the method has been demonstrated by reproducing the process. With this knowledge, a similar aging operation can be performed on any other bearing, enabling it to distinguish a completely new and approximate condition from the vibration values measured on the bearing housing. The radical difference between the initial and the final aged states suggests that a system with a similar principle, with limit monitoring, can be safely used on the asynchronous machine's bearings in the case of engine testing dynamometers.

In the future, the goal is to record a failure during the bearing operation and to develop an online status monitoring system operating on an engine testing dynamometer. For this reason, the experiments continue at the Széchenyi István University.

Acknowledgement

The authors would like to thank to EFOP-3.6.1-16-2016-00017 'Internationalisation, initiatives to establish a new source of researchers and graduates, and development of knowledge and technological transfer as instruments of intelligent specialisations at Széchenyi István University' for the support of the research.

References

1. Seker, S., A Reliability Model for Induction Motor Ball Bearing Degradation, Electric Power Components and Systems, 2010
2. Nectoux P., Gouriveau R., Medjaher K., Ramasso E., Chebel-Morello B., Zerhouni N., Varnier C., PRONOSTIA: An experimental platform for bearings accelerated degradation tests, HAL archives-ouvertes, 2012
3. Seyfettin Erbay A., Multi-Sensor Fusion for Induction Motor Aging Analysis and Fault Diagnosis, Doctoral Dissertations, 1999
4. Seker, S., Dikun, J., A redundant wavelet transform for vibration signals in electric motors, ISMA-USD, Leuven, Belgium, 2014, 429-436
5. The Institute of Electrical and Electronics Engineers, Inc, IEEE Standard Test Procedure for Thermal Evaluation of Systems of Insulating Materials for Random Wound AC Electric Machinery, IEEE

Std 117-1974, American National Standards Institute, New York, USA,
(1974)

Lifelike problems in mathematics lessons

N. Kulcsár

Széchenyi István University, Department of Mathematics and Computational Sciences

Egyetem tér 1, 9026 Győr, Hungary
e-mail: kulcsar.narcisz@math.sze.hu

Abstract: Mathematics is taught among basic courses for engineers in higher education. Since mathematics is an applied science, so teachers need to keep not only theoretical knowledge but applications in the foreground. Some simple lifelike problems are listed in this article which can connect an abstract science with real life.

Keywords: *lifelike problems, word problems, mathematics, higher education, engineering*

1. Introduction

One of the aims of higher education is to enhance the employability of the students. Higher education tries to help students to prepare for transition to the workplace. The transition cannot be successful without efficient transfer of knowledge.

In education transfer of knowledge refers to learning in one context and applying it to another, i.e. to apply acquired knowledge and skills to new situations. The transfer of knowledge in the area of mathematics is a worldwide researched area, thinking of PISA (Programme for International Student Assessment) and PIAAC (Programme for the International Assessment of Adult Competencies) researches.

2. Transfer from learning to application with lifelike problems

2.1 Transfer of knowledge

Three kind of transfer can be distinguished: from prior knowledge to learning, from learning to new learning, and from learning to application [1].

Mathematics is an applied science, hence the transfer from learning to application becomes important. There are different kind of pedagogic strategies which could help the transfer: e.g. project-oriented learning, participatory learning, some

strategies based on metacognition, problem-based learning. Some of these strategies use lifelike problems to support the transfer.

2.2 Lifelike problems

As engineers solve real-life problems in their daily work their education should be practice-oriented full of lifelike problems which are capable to connect an abstract science with real life. Lifelike mathematics problems are drawn always as word problems connected to other disciplines. Sometimes it is not easy to find a lifelike problem which contains only basic knowledge from different areas and fits to the current comprehension of students.

3. Some examples for engineers in basic mathematics courses in higher education

- I. In an electronic circuit (in order: E , r , R) the voltage (E) and resistance (r) are constant. R is the resistance of a load. The electric current (i) is given by $i = E/(r+R)$ and the power (P) delivered to the load is given by $P = Ri^2$. Resistance and load are positive. What is the value of the load (R) when the power delivered to the load is maximum?
- II. Take a slider-crank mechanism with a crank radius of r , the length of the connecting rod is denoted by l . The crank-shaft of the slider crank mechanism rotates with an angular velocity of $\omega = 1$ around the point O , point B of the connecting rod slides along the y axes. The connecting rod of the slider-crank mechanism performs a sweeping motion around point B , which results in large angular accelerations along the connecting rod. This angular acceleration multiplied by the mass of the connecting rod causes a distributed load perpendicular to the connecting rod. This distributed load tries to bend the connecting rod. Find the extrema of the angular acceleration of the connecting rod. [2]
- III. A military thread crossed over a bridge during keeping pace. The bridge collapsed. What happened?
- IV. Take a flexible chain of uniform linear mass density. Suspend it from the two ends. What is the curve formed by the chain? [3]

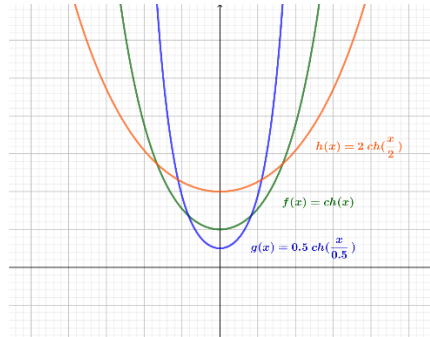


Figure 1. Catenaries with different parameters

4. Summary

It is essential to present some lifelike problems in mathematics lessons in higher education which support to connect theory with practice. Lifelike problems not only contribute to reinforce the transfer of knowledge, but also greatly contribute to enhance the motivation of students.

Acknowledgement

The author would like to thank to EFOP-3.6.1-16-2016-00017 ‘Internationalisation, initiatives to establish a new source of researchers and graduates, and development of knowledge and technological transfer as instruments of intelligent specialisations at Széchenyi István University’ for the support of the research.

References

1. Simons, PRJ, Transfer of learning: paradoxes for learners, International Journal of Educational Research, Vol. 31, No. 7. (1999), pp. 577-589.
2. Nárcisz Kulcsár, Engineering problems in mathematics lessons in higher education, in: Klara Cermakova (Ed.), 3rd Teaching & Education Conference, Barcelona, 2016, pp. 147-153.
3. G. Bognár, B. Illés, Mathematics in engineering education, in: Zenon J. Pudlowski (Ed.), 3rd WIETE Annual Conference on Engineering and Technology Education, Pattaya, Thailand, 2012, pp. 44-49.

Availability of rare earths and the need of the automotive industry

A. Buruzs

**Széchenyi István University, Department of Environmental Engineering
Egyetem tér 1, 9026 Győr, Hungary
e-mail: buruzs@ga.sze.hu**

Abstract: Mathematics is taught among basic courses for engineers in higher education. Since mathematics is an applied science, so teachers need to keep not only theoretical knowledge but applications in the foreground. Some simple lifelike problems are listed in this article which can connect an abstract science with real life.

Keywords: *rear earth metals, scarce resources, raw materials, peak of resource, electric cars*

1. Introduction

Due to the growing population of the world, the rise in the level of GDP and the changing lifestyle, the level of consumption will rise globally - resulting in higher demand for resources. Governments and companies are increasingly aware of the importance and urgency of both renewable energy sources and renewable natural resources, including energy, water, land and minerals. The interactions between resources are strong, which means that the causes of both shortages and solutions are complex. The line between "just in time" and "just not there" is very thin.

2. Population Explosion and Resource Demand

Some of our energy and raw materials (metals, elements) will be threatened in the next few decades, most of them in the next few centuries will be threatened by exhaustion. Exhaustion suggests that the materials that the current society relies on will be available in limited quantities. So they reach the limit of scarcity, so they will not be available in sufficient quantities for mass production. The material streams that are currently being met from fossil sources are diminishing, and material prices are escalating. Therefore, the future resource supply situation becomes unsustainable if resource consumption continues in line with the current trend. Governments' main task is to create a legal framework that closes material

cycles, optimizes energy use and minimizes irreversible losses as quickly as possible.

3. Danger of exhaustion and resource scarcity

The *peak of resource x (peak resource)* means that the output of resource x increases exponentially until it reaches its maximum and then the yield gradually decreases until the available set is reduced to insignificant amount. We would like to clarify some of the concepts of resource extraction at the beginning:

Time to scarcity: The time when the stock falls below 10%.

MROI (material return on investment): how much material should be invested to extract one unit of material. If the recovered material is less than that to be invested, then the extraction must be stopped.

$MROI = (\text{investment income} - \text{investment costs}) / \text{investment costs}$

Depletion of stocks is to be found in the scarcity of resources, in cases of others are poor markets and bad policies are more important factors. Even if global reserves are sufficient to meet growing demand in the coming decades, these reserves are not evenly distributed around the world; but only in a limited number of countries.

The European Union has launched a number of initiatives to mitigate the risk of scarcity of minerals and metals by requiring that the use of rare earths should be made more prudent, recycling needs to be stepped up and dealt with by developing substitutes.

According to a study by British Geological Survey [2011], in case of 27 of the 52 critical minerals and metals China is the leading exploiter. These include some strategically important metals, such as rare earth elements, which are almost exclusively mined in China [1]. Another factor contributing to the assessment of rare earth risks is that they are mined with other minerals and that rare earths are not mined on their own. Rare earths are found together in geological deposits, so the mining of individual elements is not economically efficient. Ensuring the supply of some rare earths depends on the size of geological stocks, the cost of the extraction technology used, and the price of rare earth. Finally, rare earths are subject to global control because of the environmental and social conditions in which they are mined, which further increases their risk of supply (Alonso et al. 2012). The future availability of rare earths is a cause for concern due to monopolistic supply conditions, environmentally unsustainable mining practices and rapid demand growth.

Unlike their names, rare earths [4] are not uncommon; occur in relatively large quantities in the earth's crust. However, due to their geochemical properties, they

are generally scattered and rarely found in the form of concentrated and economically exploitable form. Rare earths play a special role in the formation of magmatic rocks. Because of their ion rates, they accumulate almost uniformly in the last crystallizing and first melting component.

The most important problem with the availability of rare earths is not their geophysical abundance or scarcity, but rather whether the rare earth supply base can expand at a satisfactory pace to meet future demand, especially for some rare earths. The commercial importance of rare earths is not reflected in the quantities in which they are extracted; their annual primary production volume is approx. two orders of magnitude smaller than copper and four orders of magnitude smaller than iron (Alonso et al. 2012).

4. Field of application of rare earth elements

The rare earth metals are important because they have a critical role in many applications and are used in relatively large quantities in key technologies that are developed for sustainable mobility and energy supply.

Increased concerns about the environmental impact and reliability of fossil fuels encourage the deployment of emerging technologies such as photovoltaic, fuel cell and wind turbine. The availability of materials for these technologies is a cause for concern. Accepting new technologies can lead to a rapid change in material demand. Increased use of wind and electric vehicles is one of the most important elements of a more sustainable future. However, since the current technology of electric vehicles and wind turbines is highly dependent on rare earth elements, the future adoption of these technologies could result in a disproportionate increase in demand for these elements.

A large number of rare earths are used in the production of electric cars, which is why the stagnation of supply and the explosive growth of demand can affect manufacturers. The demand for rare earths in the world will, in a few years' time, exceed tens of thousands of tonnes if no new sites are opened. The quantities exported by China are significantly reduced because the country devotes most of its available stocks to its domestic needs. The first responses to the decline in world economic supply may come from America, with the launch of a new rare earth mine in California by 2012 [1].

In electric cars, Li-ion cells consist of a positive electrode (cathode), a negative electrode (anode), and an electrolyte. The cathode is 73% nickel, 14% cobalt, 2% aluminum, and only 11% lithium. But besides the battery, you also need to look at the electric motor that contains rare earths. Most electric car engines work with a so-called neodymium-iron-boron (NdFeB) permanent magnet, which includes iron,

copper, aluminum, cobalt, niobium, gallium, terbium, neodymium, dysprosium, and praseodymium. the three most important rare earth in our case [4].

Dysprosium can replace 0-6% of the neodymium in the magnet motor of the hybrid car. Combining this with heat treatment can increase the coercivity of the magnet. A hybrid car contains about 100 grams of dysprosium.

So it is not enough to make sure that there is enough lithium, because if we lose out of the other components, the price of the battery will go into the sky until we finally have to find another solution for storing energy [3].

Continuous improvements in the automotive industry point to a reduction in production costs, but let us not be very hopeful in the fall in the cost of alternative-driven models, which can be done in limited quantities of expensive rare earths, lithium and cobalt [2]. The availability of raw materials for electromobility remains extremely limited.

Matthias Wachter, Head of Department for Safety and Raw Materials in the German Industry Association (BDI), believes that world production of lithium was 30,000 tons in 2013 and demand would rise to 110,000 tons by 2035, demand for cobalt is currently 120-130,000 tons, and the demand for lightweight rare metals - as opposed to 28.9 thousand tonnes in 2013 - would also increase to 62.4 thousand tonnes by 2035. Insufficient availability of raw materials such as cobalt, graphite, lithium and manganese can curb the development of future technologies in Germany. Already, the demand for minerals that require a large amount of electromobility seems to be growing explosively and pushing their prices into the sky [2].

Although some raw materials are available in relatively large parts of the world, there are few countries that are ready to extract them. This is not due to the expectation of further price increases, but rather to the significant environmental impact of extraction; which greatly undermines the environmental friendliness of the technologies used in their use [2].

In addition, although recycling is limited to new waste, it is expected to change with rising prices and because applications requiring concentrated rare earths will become increasingly important. Any increase in recycling would further increase the depletion index of rare earths (reserves / current yield) (Alison et al., 2012).

The flow of material from the earth and returning to the soil through the industry has the same lifecycle as the flow of fossil fuels, with one exception: unlike fossil fuels, rare earths do not turn into flue gas after their use. They either accumulate as solid waste or regenerate and recycle them, or decompose, dust, wash, evaporate or disperse in soil, water and air.

5. Summary

As demand for rare earths is growing rapidly, prices will encourage manufacturers to reduce their net use of rare earths. This is achieved through the replacement of materials, improved efficiency and increased reuse, recycling. Due to the necessary time shift between consumption and recycling and the increasing demand for rare earths, the impact of recycling will only be significant in the long term.

Given the range of factors contributing to resource scarcity, it is clear that all actors in the supply chain should be involved in this issue. Mining companies play a key role in defining and developing new reserves and managing existing stocks; governments should remove trade barriers; universities and research institutes need to accelerate R&D; companies need to invest more in the discovery of substitutes and resource efficiency innovations, and consumers must take responsibility for recycling waste materials.

Acknowledgement

The author would like to thank to EFOP-3.6.1-16-2016-00017 ‘Internationalisation, initiatives to establish a new source of researchers and graduates, and development of knowledge and technological transfer as instruments of intelligent specialisations at Széchenyi István University’ for the support of the research.

Literature

1. British Geological Survey, ‘Risk List 2011’, 2011
2. E. Alonso, A. M. Sherman, T. J. Wallington, M. P. Everson, F. R. Field, R. Roth, and R. E. Kirchain: Evaluating Rare Earth Element Availability: A Case with Revolutionary Demand from Clean Technologies. *Environ. Sci. Technol.*, 2012, 46 (6), pp 3406–3414
3. [1] https://www.napi.hu/nemzetkozi_vallalatok/a_hibridek_miatt_dragulhatna_k_a_ritka_femek.418289.html
4. [2] http://gyartastrend.hu/autoipar/cikk/ellentmondasok_az_elektromobilitasban
5. [3] <https://villanyautosok.hu/2017/11/15/egyre-tobb-villanyauto-de-van-eleg-litium/>
6. [4] <https://hu.wikipedia.org>

Robot path generation from image recognition

N.Szántó

Széchenyi István University, Department of Automobil Production
Technology
H-9026 Győr, Egyetem tér 1. Hungary
szanto@sze.hu

Abstract: This paper contains the description of the generating a robot path with image recognition. The expectations of the system and the research step from machine vision to image processing are presented. This article does not yet contain the description of the robot path generation.

Keywords: *machine vision, digital image processing, hough transformation*

1. Introduction

The aim of the research is to detect, recognize and then trace the contour line with an industrial robot. The first task is to spot the field of machine vision, where initially only 2D shapes are detected. Then the digital image processing will determine the coordinates of the shapes, which are the necessary conditions for the robot path generation. The industrial connection point of the research is robot welding with the help of which the preparation time of the welds is expected to be greatly reduced.

2. Machine vision tools and their application

The use of machine vision can be extremely widespread. The features that can be optically detected are highly likely to be automated, so the use of this feature of machine vision is the goal. Components of a general machine vision system: illumination, camera, image processing hardware and software, and a communication interface.

Contour as input data can be done in two ways, by loading an existing image or by taking a picture. The picture can be made by using a smartphone or webcam. The sample task was based on a free contour drawn on a A4 sheet, digitized by a webcam. Image processing was performed using functions provided by OpenCV.

Because the page can be in the scanned image in any position and size, it should be dimensioned to get the correct coordinate values. The image needs to be

transformed so that the contour appears in the original orientation, that is, the sides of the page coincide with the sides of the image.

Step 1

First, we differentiate the background and the page. The image is converted into HSV (hue, saturation, value) format for saturation and, for more accurate results, to use the brightness parameters for distinction. Based on these, we create a binary image (Figure 1), that is the background is black, the page will be white to define the corner points.

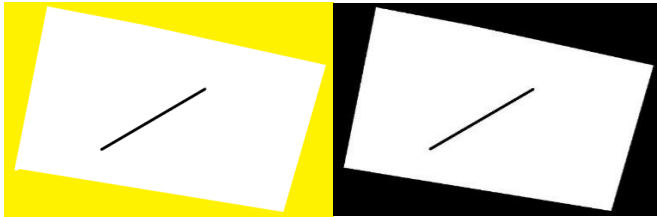


Figure 1. Background and base separation

Step 2

Finding corner points. Finding the corner points is provided by the *cornerarris* function, which examines pixels of the image in square groups, observing their intensity change (Figure 2). At corners, moving these squares of multiple pixels in any direction changes the intensity. Reduce running time by scanning larger squares first, resulting in inaccurate results. The *cornerSubPix()* function examines the environment of the previously defined points with a square of 2x2, so that the corner points are returned accurately. These results give you many points if you find corners in the shapes that appear on the image, so the points found are the closest to the corners of the image. The program calculates the distance of all found points from the corners and the closest to it is saved.

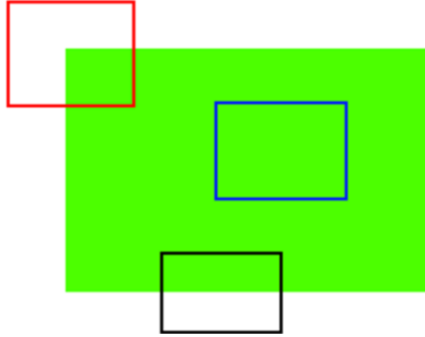


Figure 2. Finding corner points

Step 3

Photo transformation. Knowing the corner points of the page and the corners of the picture, the *getPerspectiveTransform* function creates a transformation matrix. The *warpPerspective* function performs the conversion so that the corners of the tab on the image will be in the corners of the image (Figure 3).

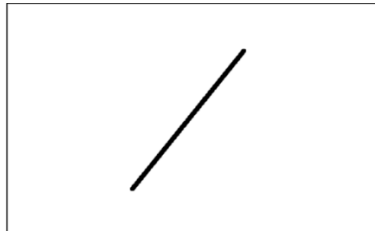


Figure 3. Transformed image

The size of the shape(s) on the picture can be determined by the size of one of an image being known. The size of the A4 sheet on which the contour is based are known, so we can determine a ratio to get the exact dimensions. This is the basis for calculating the relationship between pixels and reality dimensions.

3. Digital image processing

Image processing is done on PC, Python using OpenCV. Its basic task is the clear recognition of the shapes in such a way that later we can generate coordinates for the robot. In the first step, only the straight contours are processed. One of the algorithms used to detect straight lines in image processing is the Hough transformation.

3.1 Hough transform

In OpenCV, Hough transformation will look at white pixels, so the original image created during scaling must be binary again to isolate the background and contour. The binary image has a light background and a dark contour, and this must be inverted for the correct operation of the algorithm. After inverting, a black contour will be a white contour.

The first step of the transformation is to align straight lines to the white pixels (dots). This line is parameterized. Instead of the traditional straight equation we get a parameterized equation with an angle and distance. The equation parameters give the distance from the straight origin and the angle closed with the x -axis.

$$\rho = x \cdot \cos\theta + y \cdot \sin\theta \quad (1)$$

where:

ρ : distance between origin and the line

θ : angle between the line and the x -axis

The equation of the parameters of the equation used by Hough transformation is well defined: $\theta \in [0, \pi]$ in radians or $\theta \in [0, 180]$ degrees, and $\rho \in [-D, D]$, where D corresponds to the diagonal length of the image. One of the great advantages of Hough transformation is that the line described in the x - y plane can be described in a single point in the Hough region. An unlimited number of lines can be drawn passing through a given point. The resolution of angular position and distance parameters is 1 radian and 1 pixel. At the point, the straight line can be rotated by increments corresponding to the angle resolution until the initial angular position. Because of the discrete resolution, votes from each point are received for each parameter combination. Each line receives as many points as it fits into it, so the true pixel numbers of the straight lines can be determined (Figure 4). The endpoints of the lines can be determined by examining the pixels.

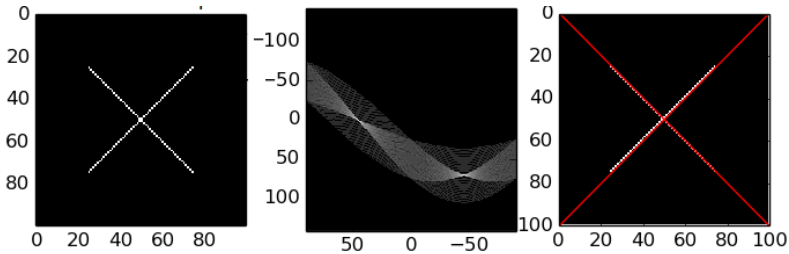


Figure 4. A binarized image (l), Hough visualization (c), discovered lines(r)

3.2 Superlines

During the Hough transformation, too many lines are detected, so perceived lines may overlap, or some sections may be missing. To solve the problem, lines that are close to each other and align with each other are grouped together. The lines are classified according to the horizontal plane or vertical orientation relative to each other and then arranged according to x, y coordinates. The lines are compared with each other, and if their distance and inclination angle are within a certain tolerance, these lines are taken into one group, each of which is equivalent to a superline. The starting and end point of the superline is the starting point of the first line within the ordered group and the end point of the last line within the group.

4. Summary

By machine vision and digital image processing, the input image was sensed and processed, from which the contours of the shapes were also defined. Thus, the input parameters required for robot programming are available. The automatic transfer of data and the transformation of the data into a robot program is the next step in the research.

Acknowledgement

The authors would like to thank to EFOP-3.6.1-16-2016-00017 ‘Internationalisation, initiatives to establish a new source of researchers and graduates, and development of knowledge and technological transfer as instruments of intelligent specialisations at Széchenyi István University’ for the support of the research.

References

1. A. Rövid, Z. Vámosy, Sz. Sergyán, A gépi látás és képfeldolgozás párhuzamos modelljei és algoritmusai, Typotex Kiadó, 2014. in Hungarian.
2. E.R. Davies, Computer and Machine Vision: Theory, Algorithms, Practicalities, 4th Edition, Elsevier, 2012.
3. S. Seitz, R. Szeliski, Computer Vision (CSE 576), University Washington, 2012.
4. Open Source Computer Vision Documentation (2018) [cited 2018-04-20]. URL: <https://opencv.org/>

Statistical Quality and Process Control with using R and Digital Twin

G. Monek

Széchenyi István University, Department of
Automobil Production Technology
H-9026 Győr, Egyetem tér 1. Hungary
monek.gergo@sze.hu

Abstract: This paper contains the description of the various statistical quality assurance procedures and their necessity. Using the methods presented can be gained extra information about manufacturing and logistics processes, which can help increase the efficiency and stability of these processes.

Keywords: *Quality control, Statistics, I4.0, R*

1. Introduction

Quality assurance is becoming more and more important today because in the fierce competitive environment the advantage can be the production of more economical and productive production logistic and other processes, the number of errors should be approximated to zero. There are several statistical based procedures for quality control, most of which can be automated and accelerated by scripts. The present article presents some of these techniques, then discusses the feasibility and usability of these techniques.

2. Description of the system components

The methods used are based on data from different processes. The data acquisition and treatment strategy should be an important part of the quality control planning, as all the subsequent activities will be based on such data. Once we have the data available, we need the appropriate computing tools to analyse them. The application of statistical methods to Quality and Process Control requires the use of specialized software. There exist a wide range of software packages for Statistics in general. Most of them include specific options for quality control, such as control charts or capability analysis. Even some of them are focused on quality tools. R is a free software environment for statistical computing and graphics. It compiles and runs on a wide variety of platforms. R is an integrated suite of

software facilities for data manipulation, calculation and graphical display. Among other things it has

- an effective data handling and storage facility,
- a suite of operators for calculations on arrays, in particular matrices,
- a large, coherent, integrated collection of intermediate tools for data analysis,
- graphical facilities for data analysis and display either directly at the computer or on hardcopy, and
- a well developed, simple and effective programming language which includes conditionals, loops, user defined recursive functions and input and output facilities.

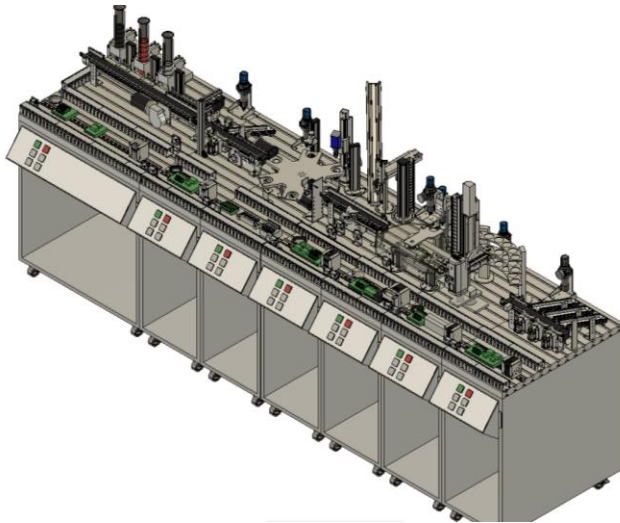


Figure 1. Festo Prolog Factory (CAD model)

The precondition for preparing the automated quality and process control model is to know the structure, components and their relationships, operating conditions, communication and control of the existing resource. At the sample production line, there are nine modular cells (Figure 1) where three types of products can be manufactured. Each cell has a separate PLC control, through sensors and actuators a linear flow is realized between the stations. As the physical system does not collect and is not capable of collecting data correctly, the system's digital twin can be used for data collection.

The digital model is a duplicate of the physical system, with some differences that it is possible to exploit the possibilities offered by the simulation environment, and can also be used to gather various additional information. In this way, there is a greater amount of data and/or more data available for quality and process control techniques. [1] [2] [3]

3. Possible architecture

A MES system running control and monitoring over real and digital models would also collect and store various log data. Scripts created based on quality assurance techniques work from these data and the processed information is sent to the user through a web-based graphical interface (Figure 2). The interface allows the user to view graphically the desired queries in almost real-time. In the event that a user perceives an intervention in the process as required by the statements, user can make modifications.

Some of possible methods:

- Control charts
- Process capability
- Pareto analysis
- Cause and effect diagram

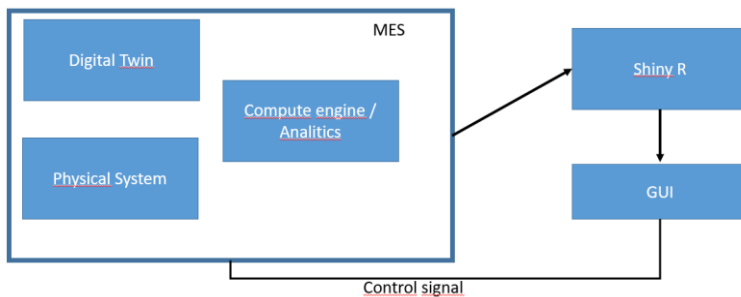


Figure 2. An outline of a possible architecture

4. Summary

From many locations, a variety of data can be collected in a modern factory. Collecting data is just a little bit of the whole, since these data are useful if they are easily interpretable and meaningful. With the help of the presented architecture can be created a user-friendly environment for data visualization. Enabling it to accelerate and fine-tune most of today's quality assurance methods. The next step

of the research building an architecture is to incorporate a learning algorithm to reduce the number of user decision-making and achieve a higher level of autonomy.

Acknowledgement

The authors would like to thank to EFOP-3.6.1-16-2016-00017 ‘Internationalisation, initiatives to establish a new source of researchers and graduates, and development of knowledge and technological transfer as instruments of intelligent specialisations at Széchenyi István University’ for the support of the research.

References

1. Cano, Emilio L., M, Moguerza, Javier, Prieto Corcoba, Mariano: Quality control with R, Springer, 2015
2. Schober, Manual prolog-factory, Festo Didactic GmbH & Co.KG, Denkendorf, 2010
3. Peter Clount, Janarde Lepore: Importance of Quality Historical Data Plant Operation and Advanced Process Control Implementation, 16th IFAC Symposium, 2013

Experimental Investigation of the Friction Decreasing Effects of Nanosized C₆₀ Fullerene Doped Engine Lubricant Performed on Oscillating Tribometer

Á. I. Szabó¹, Cs. Tóth-Nagy¹

¹Széchenyi István University. Department of Internal Combustion Engines
H 9026 Győr, Egyetem sq. 1.,
e-mail: toth-nagy.csaba@sze.hu

Abstract: This article presents the experimental investigation and test results of nanosized C₆₀ fullerene used as additive in engine lubricating oil on oscillating tribometer. The article presents the test equipments, the method for the investigation, the roles of the fullerene molecules in the tribosystem, and the results of the experiments. The article concludes that fullerene easily dissolves in engine lubricant, and reduces the friction by 4-8%.

Kulcsszavak: fullerén, nanoadalék, tribométer, motorolaj, súrlódás

1. Bevezetés

Napjaink motorolajai speciálisan megtervezett komponensei a belsőégésű motoroknak. A motorolaj csökkenti a súrlódást az érintkező alkatrészek között, ezáltal közvetve csökkenti – az autóipar két legégetőbb problémáját - a tüzelőanyag-fogyasztást és a CO₂ emissziót. Megfelelő, multifunkcionális motorolajok kifejlesztéséhez a gyártók az alapolajon kívül számos kémiai adalékot használnak. A nanoadalékok azok a legfeljebb 100 nm nagyságú adalékok, melyek méretükből kifolyólag könnyedén behatolhatnak a kontaktfelületek közé egy tribológiai rendszerben. Bizonyos nanoadalékok kopáscsökkentő hatása meghaladja a jelenleg széles körben alkalmazott kémiai adalékokét, az egyik ilyen adalék lehet a C₆₀-as fullerén. Tudományos publikációk jelentései szerint különböző nanoméretű porok – köztük a C₆₀-as fullerén – képesek betölteni a súrlódáscsökkentő kémiai adalékok szerepét a motorolajba keverve [1]. Jaekun és Kwangho 2009-ben megerősítették a C₆₀ fullerén súrlódáscsökkentő hatását olajba keverve. Jelentésük szerint a súrlódáscsökkentő hatás alacsony terheléseken (<1600 N) a legjobb [2] és egyes munkapontokban a csökkenés mértéke akár 90%

is lehet [3]. 2014-ben Meibo 12-19%-os súrlódáscsökkenésről publikált C60 fullerénnel adalékolt hűtőgépolajok esetében [4].

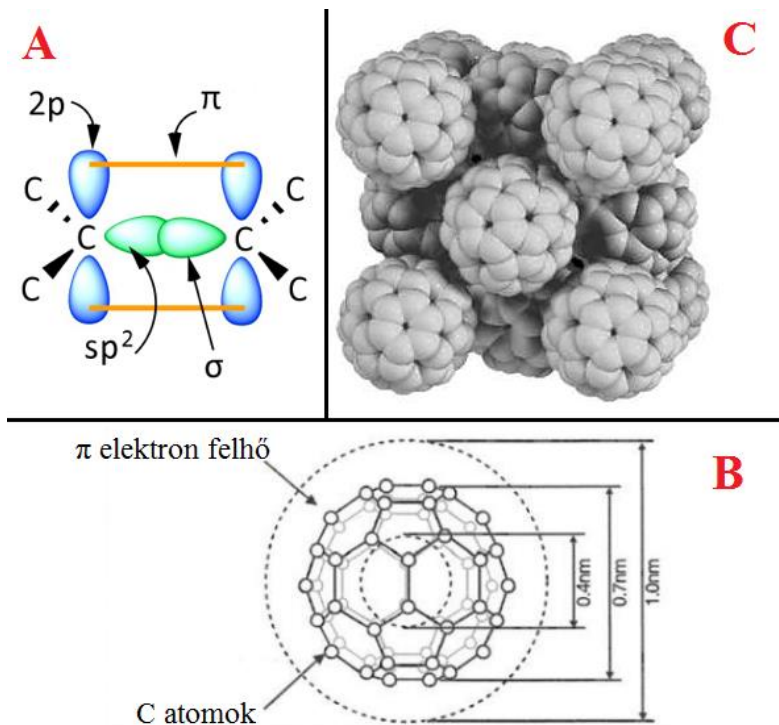
2. Mérések előkészítése

2.1 Fullerén

A mérések során alkalmazott >99,5%-os tisztaságú C60-as fullerén (CAS 99685-96-8) olyan gömb alakú molekula, melyben a 60 darab szénatom elrendeződése futball labdára emlékeztet. 1985-ös felfedezése óta kutatások középpontjában áll, alakja, magas keménysége, csapdázási képessége, mechanikai-, elektromos- és kémiai tulajdonságai miatt. Súrlódáscsökkentő hatásának alapja az alkotó szén atomok közti kapcsolatból származik. A szén atomok sp^2 hibrid kovalens kötéssel kapcsolódnak egymáshoz, mely a legerősebb ismert kötés a szilárd anyagokban (1a. ábra). Az sp^2 hibrid kötés π -kötései kiemelkednek a kötést alkotó atomok síkjából, tehát a kötés egyik fele a fullerén belsejében, míg másik felük a fullerén felületén alakul ki. Faraday kalitkája szerint ezek a π -orbitálon kötő elektronok főként a fullerén külső részén levő térben tartózkodnak, ez egy külső elektronszférahoz létre a fullerén körül (1b. ábra). A fullerén külső elektronszféraja és magas keménysége miatt többféle súrlódáscsökkentő szerepet tölt be egy tribológiai rendszerben.

2.2. Kenőolaj előkészítés

A mérésekhez használt kenőolaj alapjául a „Castrol EDGE 0W30 boosted with TITANIUM FST” szintetikus motorolaj szolgált. Négy különböző keverék került meghatározásra a mérésekhez, a fullerén tömegaránya alapján az olajban. Referencia mérés, melyben nincsen hozzáadott fullerén, 0,05; 0,1 illetve 0,25 tömegszázalék arányban. Az alkalmazott fullerén örölt kristályos fullerit formában volt – ami a fullerén kristályos formája – melyben az egyes fullerén molekulákat gyenge van der Waals erők tartanak össze, ilyen fullerit szerkezetet mutat az 1c. ábra. Miután a meghatározott mennyiségű fullerén az olajba került, az egyes fullerén molekulák szétválasztásáért és a homogén eloszlásáért a keverék ultrahangos tisztító berendezésbe került. Az ultrahangos tisztító nagy frekvenciájú (20-400 kHz) hanghullámokkal kavitációt hozott létre az olajban és fellazította a fullerén agglomerációkat. Bár a C60 fullerén korlátozottan oldódik a szintetikus motorolajok fő összetevőjében (poli- α -olefin), a keverékben levő fullerén nagyobb részét viszont a motorolaj diszpergens tartalma tartotta szuszpenzióban.



1. ábra: a) sp^2 hibrid kovalens kötés; b) C_{60} fullerén molekula felépítése és méretei; c) fullerén molekulákból felépülő fullerit kristályrács.

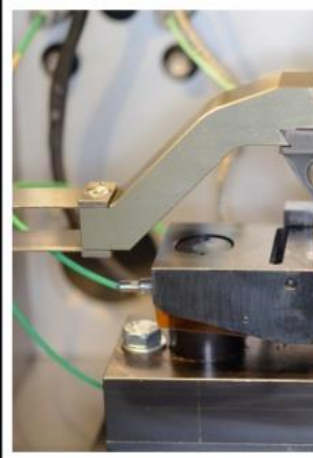
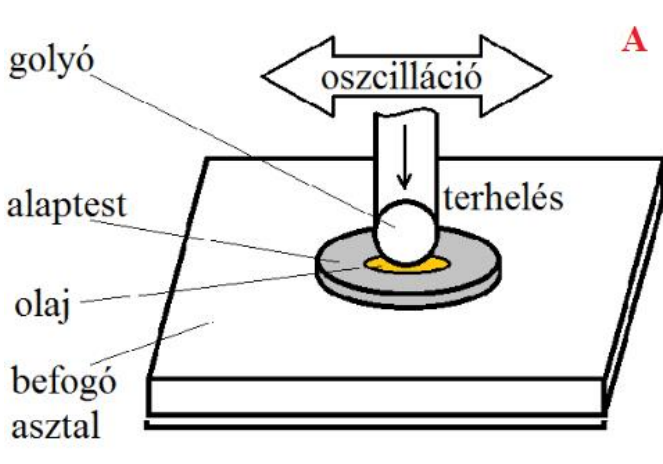
2.3. Tribométer

A mérések a győri Széchenyi István Egyetem oszcilláló tribométerén történtek. Az oszcilláló tribométer működési elve egy álló alaptest és egy arra merőlegesen rányomott lineáris oszcilláló mozgást végző golyó egymáshoz képesti elmozdulásán alapul, ezt mutatja a 2a. ábra. Az összerakott oszcilláló tribométert a 2b. ábra mutatja. A mérés előtt előre meghatározott mennyiségű - egy csepp - olaj került az alaptest és a golyó közé, a kontaktfelületekre, ez az olaj keneti a felületeket a mérés folyamán. A tribométer felfűtötte a teljes rendszert $100\text{ }^\circ\text{C}$ fokra, ezután kezdődött el a golyó mozgása és a mérés. A mérés első 30 másodpercében a tribométer egy bejáratást végzett a próbatesteken alacsonyabb, 50 N normálerővel, majd a továbbiakban a mérés során 200 N nagyságú normálerő mellett a golyó frekvenciája 50 Hz volt, 1 mm hosszúságú löketen. A mérések során használt súrlódó testek (csapok, tárcsák, golyók, alaptestek) azonos anyagból, 100Cr6 jelölésű csapágyacélból készültek. A 2 órás mérés során az érintkező felületek

bejártak és kialakult rajtuk egy tribológiai határreteg, az úgynevezett tribofilm. A súrlódás megállapításához a mérések során folyamatosan rögzítette a tribométer a pillanatnyi súrlódást. A mérési paramétereket az 1. táblázat foglalja össze. Az azonos keverékekkel történő mérések átlagának, az utolsó 2 perces átlagos súrlódásnagysága határozta meg az adott keverékhez tartozó súrlódási együttható értékét.

1. táblázat: Mérési paraméterek a bejártatás és a mérés fázisaiban.

	bejártatás	mérés
normálerő	50 N	200 N
frekvencia	50 Hz	50 Hz
lökethossz	1 mm	1 mm
hőmérséklet	100 °C	100 °C
időtartam	0-30 s	30-7200 s

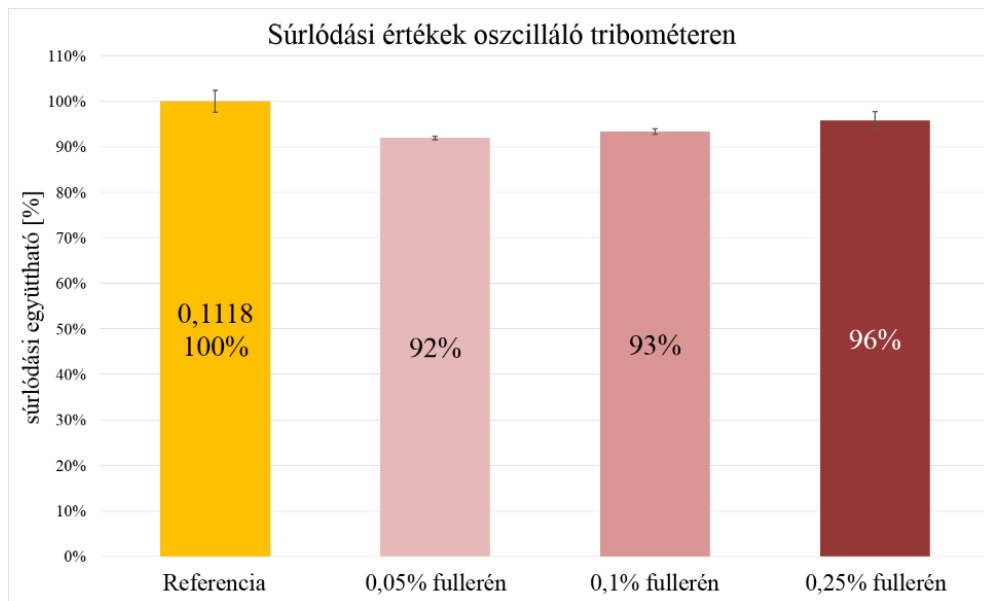


2. ábra: A mérések során alkalmazott tribométer mérésre készen összeszerelve, illetve sematikus felépítése (a és b ábra).

3. Mérési eredmények

A mérés célja a C₆₀ fullerénnel adalékolt és a referencia motorolaj súrlódási együtthatóinak összehasonlítása. A csap-tárcsás tribométeren végzett mérések

esetében, megállapítható, hogy a fullerén minden alkalmazott koncentrációban 4-8%-os súrlódáscsökkenést mutatott a referencia mérésekhez képest, ezt a 3. ábra mutatja. Az oszcilláló tribométeren végzett mérések hasonló értékeket mutattak, mint a csap-tárcsás tribométeren végzett mérések. Megállapítható, hogy a C₆₀-as fullerén mindhárom kísérleti koncentrációban 4-8%-os súrlódáscsökkenést mutatott a referencia értékhez képest, illetve az egyes keverékekkel végrehajtott kísérletek szórását (3. ábra).



3. ábra: Átlagos súrlódási együttható az oszcilláló tribométeren végzett mérések utolsó 2 percében.

3.1 Eredmények kiértékelése

A fullerén súrlódáscsökkentő hatásának oka, hogy az olajban szuszpendált ~1 nm átmérőjű fullerén molekulák könnyen bejutnak a kontakt régióba. Magas keménysége és morfológiája miatt „golyóscsapágyként” funkcionál a súrlódó felületek között, illetve csökkenti a fém-fém kontaktok arányát és az azzal járó adhezív kopást [2]. Magas keménysége miatt képes polírozni a felületet az érdességi csúcsok csökkentésével. Kutatások igazolják, hogy a fullerén magas felületi nyomás és hőmérséklet hatására képes beágyazódni a súrlódó alkatrészekbe, illetve a tribofilm komponensévé válni [1]. A fulleréntartalmú tribofilm magasabb keménységű, kopásállóbb és a fullerének külső elektronhéja

miatt könnyebben mozdulnak el egymáson az ilyen tribofilmek. A C_{60} -as fullerén sűrűlódáscsökkentő viselkedését a jelen mérések megerősítik.

4. Konklúzió

A jelen értekezés megvizsgálta a C_{60} fullerén mint nanoméretű motorolaj adalék hatását a sűrűlódási együtthatóra oszcilláló tribométeren. A mérések eredményeiből megállapítható, hogy a fullerén sűrűlódáscsökkentő hatása 4-8% közé tehető. Ennek magyarázata a C_{60} molekula gördülőelemként és tribofilm komponensként való viselkedése áll.

Acknowledgement

The authors would like to thank to EFOP-3.6.1-16-2016-00017 'Internationalisation, initiatives to establish a new source of researchers and graduates, and development of knowledge and technological transfer as instruments of intelligent specialisations at Széchenyi István University' for the support of the research.

Hivatkozások

1. Wei Dai et al.; Roles of nanoparticles in oil lubrication; Tribology International, Elsevier, 2016, 102, 88-98.
2. Jaekeun Lee et al.; Application of fullerene-added nano-oil for lubrication enhancement in friction surfaces; Tribology International, Elsevier, 2009, 42, 440-447.
3. Kwangho Lee, Jaekeun Lee, et al.; Performance evaluation of nano-lubricants of fullerene nanoparticles in refrigeration mineral oil; Current Applied Physics, Elsevier, 2009, 9, 128-131.
4. Meibo Xing et al.: Application of fullerene C_{60} nano-oil or performance enhancement of domestic refrigerator compressors; International Journal of Refrigeration, Elsevier, 2014, 40, 398-403.